AGU PUBLICATIONS

Paleoceanography

RESEARCH ARTICLE
10.1002/2015PA002881

Key Points:
- Eleven late Miocene-early Pliocene oxygen isotope events and four long-term trends are identified
- Cryosphere/carbon cycle sensitivity and Earth System Response define climate variability
- Dynamic and stable states characterized by ice volume extent and variability are identified

Supporting Information:
- Texts S1–S3 and Figures S1–S9
- Tables S1–S7

Correspondence to:
A. J. Drury,
ajdrury@marum.de

Citation:
Drury, A. J., C. M. John, and A. E. Shevenell (2016), Evaluating climatic response to external radiative forcing during the late Miocene to early Pliocene: New perspectives from eastern equatorial Pacific (IODP U1338) and North Atlantic (ODP 982) locations, *Paleoceanography*, *31*, doi:10.1002/2015PA002881.

Received 14 SEP 2015
Accepted 15 DEC 2015
Accepted article online 18 DEC 2015

Evaluating climatic response to external radiative forcing during the late Miocene to early Pliocene: New perspectives from eastern equatorial Pacific (IODP U1338) and North Atlantic (ODP 982) locations

Anna Joy Drury[1,2], Cédric M. John[1], and Amelia E. Shevenell[3]

[1]Department of Earth Science and Engineering, Imperial College London, London, UK, [2]Now at MARUM – Center for Marine Environmental Sciences, University of Bremen, Bremen, Germany, [3]College of Marine Science, University of South Florida, St. Petersburg, Florida, USA

Abstract Orbital-scale climate variability during the latest Miocene-early Pliocene is poorly understood due to a lack of high-resolution records spanning 8.0–3.5 Ma, which resolve all orbital cycles. Assessing this variability improves understanding of how Earth's system sensitivity to insolation evolves and provides insight into the factors driving the Messinian Salinity Crisis (MSC) and the Late Miocene Carbon Isotope Shift (LMCIS). New high-resolution benthic foraminiferal *Cibicidoides mundulus* $\delta^{18}O$ and $\delta^{13}C$ records from equatorial Pacific International Ocean Drilling Program Site U1338 are correlated to North Atlantic Ocean Drilling Program Site 982 to obtain a global perspective. Four long-term benthic $\delta^{18}O$ variations are identified: the Tortonian-Messinian, Miocene-Pliocene, and Early-Pliocene Oxygen Isotope Lows (8–7, 5.9–4.9, and 4.8–3.5 Ma) and the Messinian Oxygen Isotope High (MOH; 7–5.9 Ma). Obliquity-paced variability dominates throughout, except during the MOH. Eleven new orbital-scale isotopic stages are identified between 7.4 and 7.1 Ma. Cryosphere and carbon cycle sensitivities, estimated from $\delta^{18}O$ and $\delta^{13}C$ variability, suggest a weak cryosphere-carbon cycle coupling. The MSC termination coincided with moderate cryosphere sensitivity and reduced global ice sheets. The LMCIS coincided with reduced carbon cycle sensitivity, suggesting a driving force independent of insolation changes. The response of the cryosphere and carbon cycle to obliquity forcing is established, defined as Earth System Response (ESR). Observations reveal that two late Miocene-early Pliocene climate states existed. The first is a prevailing dynamic state with moderate ESR and obliquity-driven Antarctic ice variations, associated with reduced global ice volumes. The second is a stable state, which occurred during the MOH, with reduced ESR and lower obliquity-driven variability, associated with expanded global ice volumes.

1. Introduction

The latest Miocene (8.0–5.33 Ma) to early Pliocene (5.33–3.50 Ma) is one of the most climatically stable periods of the Cenozoic, characterized by minor long-term (>1 Myr) cooling and ice growth, followed by climatic warming [*Zachos et al.*, 2001]. These long-term trends are punctuated by the Late Miocene Carbon Isotope Shift (LMCIS, 7.6–6.6 Ma) and the Messinian Salinity Crisis (MSC, 5.96–5.33 Ma), which have been attributed to changes in the carbon cycle and ocean circulation, and global sea level variations related to changing ice volume [*Hodell et al.*, 1994, 2001; *Bickert et al.*, 2004; *van der Laan et al.*, 2005, 2006; *Hodell and Venz-Curtis*, 2006; *Ohneiser et al.*, 2015]. However, the evolution of orbital-scale (<400 kyr) ice volume and carbon cycle variability remains unknown, due to the absence of high-resolution deep-sea benthic foraminiferal $\delta^{18}O$ and $\delta^{13}C$ records and well-dated ice-proximal records from Antarctica's continental margins [*Naish et al.*, 2009] between 8.0 and 6.0 Ma.

External radiative forcing is an important influence on orbital-scale climate variability, which can be assessed using Earth system sensitivity, e.g. the change in temperature with a doubling of atmospheric CO_2 [*Pagani et al.*, 2009; *Rohling et al.*, 2012; *Royer et al.*, 2012]. Another approach is to investigate the sensitivity of individual feedback systems of the Earth's climate, including the cryosphere and carbon cycle, to radiative forcing [*Pisias et al.*, 1995]. Increased climate sensitivity typically leads to greater variability in feedback systems.

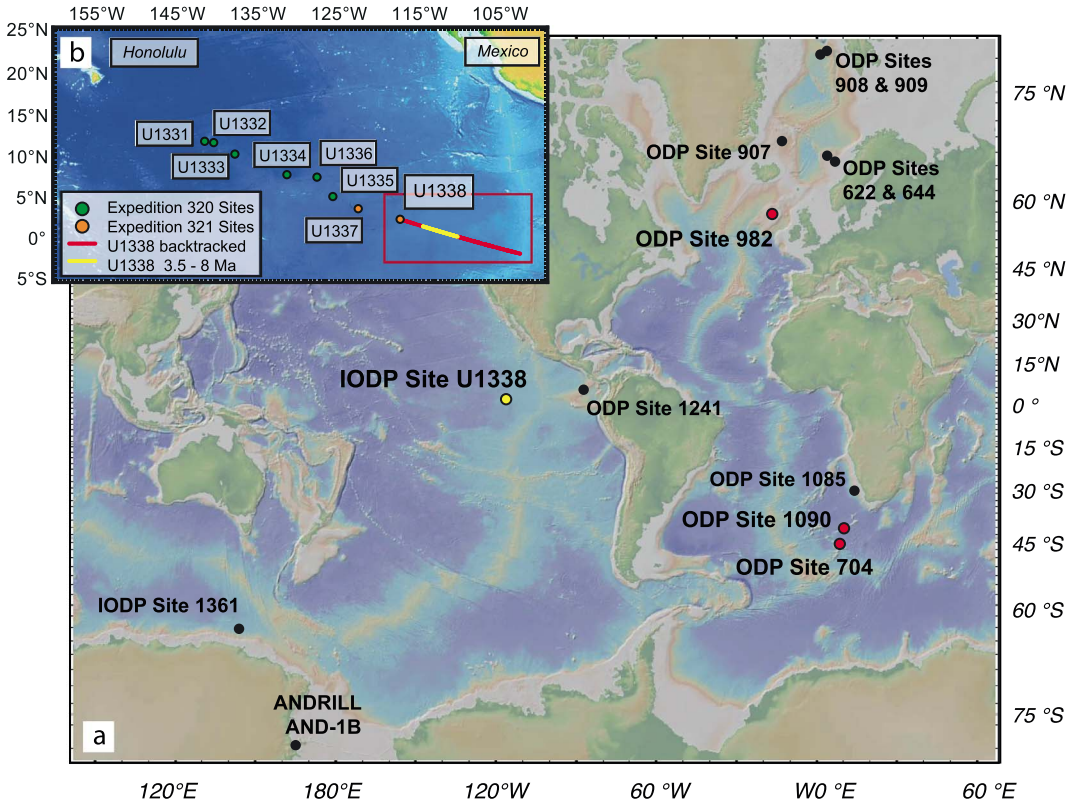

Figure 1. Site overview. (a) Dots show the location of the sites discussed in this study. New records generated in this study are shown in yellow. (b) Insert shows the location of the IODP PEAT Expedition 320/321 sites. The backtracked location of Site U1338 is shown as a red line. The target interval between 8.0 and 3.5 Ma is shown in yellow (GeoMapApp) [*Ryan et al.*, 2009].

Here we investigate global changes in late Miocene to early Pliocene cryosphere and carbon cycle sensitivity and qualitatively assess Earth's climate response to changes in radiative forcing, defined here as the Earth System Response (ESR). To achieve this, we (1) generate new high-resolution benthic foraminiferal $\delta^{18}O$ and $\delta^{13}C$ records in the eastern equatorial Pacific; (2) establish a high-resolution chronology and improve the stable isotope stratigraphy between 8.0 and 3.5 Ma; (3) use benthic $\delta^{18}O$ and $\delta^{13}C$ variability to qualitatively estimate cryosphere/carbon cycle sensitivity and ESR; and (4) assess changes in cryosphere/carbon cycle sensitivity and ESR in the context of late Miocene to early Pliocene climate evolution. By evaluating the temporal evolution of Earth's response to external radiative forcing during a period of relative long-term climatic stability, we gain insight into the forcings and feedbacks associated with the LMCIS and MSC.

2. Materials and Methods

2.1. International Ocean Drilling Program Site U1338 (Eastern Equatorial Pacific) Paleoceanographical Setting

Geochemical records from the equatorial Pacific provide a good approximation of the mean global climate state, due to the large size of the Pacific Ocean $\delta^{18}O$ and $\delta^{13}C$ reservoirs [*Lyle et al.*, 2010]. Due to abundant biogenic calcite ($CaCO_3$) and high continuous sedimentation rates, International Ocean Drilling Program (IODP) Site U1338, in the eastern equatorial Pacific, is an ideal location for generating the high-resolution $\delta^{18}O$ and $\delta^{13}C$ records required (Figure 1 and supporting information Table S1; water depth: 4200 m, paleodepth: ~3850–4050 m) [*Expedition 320/321 Scientists*, 2010; *Pälike et al.*, 2010]. During the late Miocene to early Pliocene, Site U1338 was located in the 0–2°N equatorial Pacific productivity zone, above the calcite compensation depth [*Pälike et al.*, 2012]. The first-order shipboard paleomagnetic and nannofossil datum-based age model (Figure 2 and supporting information Table S2a) indicates that a continuous composite section of expanded late Miocene and Pliocene calcareous nannofossil ooze with siliceous microfossils-rich intervals was recovered between 48 and 180 m core composite depth below seafloor (CCSF-A) [*Expedition 320/321 Scientists*, 2010; *Wilkens et al.*, 2013].

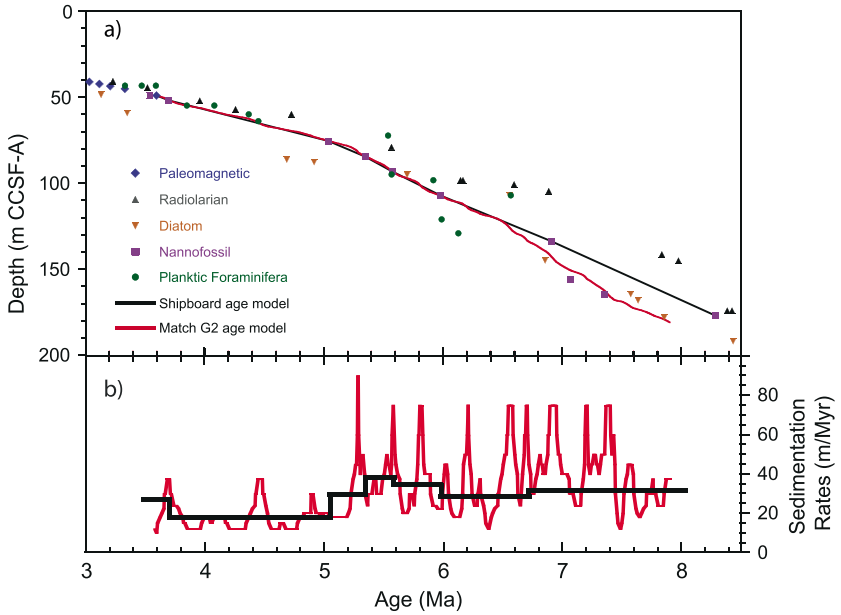

Figure 2. Age models and sedimentation rates. (a) Age-depth relationships for the shipboard (black) and second-generation (G2) Match (red) age models, together with the shipboard biostratigraphic/paleomagnetic datums. (b) Sedimentation rates for the first-order (black) and second-generation Match (red) age models.

Sedimentation rates average 28.7 m/Myr in the late Miocene and 12.7 m/Myr in the early Pliocene. The weight percent $CaCO_3$ is ~70–80%, decreasing to ~40–60% in discrete intervals [*Lyle et al.*, 2012; *Lyle and Backman*, 2013]. Benthic foraminifera are well preserved, with evidence of only minor calcite overgrowth and dissolution [*Drury et al.*, 2014].

2.2. IODP Site U1338 Benthic Foraminiferal $\delta^{18}O$ and $\delta^{13}C$ Records

We collected 1330 samples every 10 cm along the revised splice (time step equivalent: late Miocene ~3.5 kyr; early Pliocene ~7.9 kyr) [*Wilkens et al.*, 2013], to resolve all late Miocene orbital cycles and early Pliocene obliquity and eccentricity. Samples were freeze dried, wet sieved at 63 μm, and oven dried at 45°C. Oxygen ($\delta^{18}O$) and carbon ($\delta^{13}C$) isotope ratios were analyzed on three to six 250–500 μm translucent benthic foraminifera *Cibicidoides mundulus* (*C. mundulus*) tests, which were ultrasonicated in methanol to remove fine-grained particles: 11% of the data set utilizes additional 125–250 μm tests, but no isotope offset was observed between size fractions (supporting information Table S3).

Most samples were analyzed for stable isotopes using a Kiel IV attached to a Thermo Mat 253 (70°C 105% H_3PO_4) in the Qatar Stable Isotope Laboratory at Imperial College London (ICL); 7% were analyzed via a GasBench II attached to a continuous-flow Thermo DeltaPLUS XP in the Bloomsbury Environmental Isotope Facility at University College London (UCL; 70°C 100% H_3PO_4). Analytical precision was 0.07‰ for $\delta^{18}O$ and 0.04‰ for $\delta^{13}C$ at ICL and 0.09‰ for $\delta^{18}O$ and 0.02‰ for $\delta^{13}C$ at UCL. Repeat analyses of samples and ICL's Carrera Marble standard indicated no offset between laboratories. Sample reproducibility (12%) for ICL data was better than 0.07‰ for $\delta^{18}O$ and 0.08‰ for $\delta^{13}C$, and for UCL data equal or better than the analytical precision. We added 0.64‰ to *C. mundulus* $\delta^{18}O$ to reflect equilibrium calcite $\delta^{18}O$ [*Shackleton et al.*, 1995].

2.3. Stratigraphic Correlation Using "Match"

We developed high-resolution age control at Site U1338 using biostratigraphic age datums and stratigraphic correlations to the North Atlantic Ocean Drilling Program (ODP) Site 982, which has continuous, high-resolution astronomically tuned isotope records (Figure 1 and supporting information Table S1; water depth: 1134 m) [*Jansen and Raymo*, 1996; *Shipboard Scientific Party Exp.*162, 1996; *Hodell et al.*, 2001; *Hodell and Venz-Curtis*, 2006]. We correlated the two sites using the Match software program [*Lisiecki and Lisiecki*, 2002; *Lisiecki and Herbert*, 2007], which aligns target and signal data sets to generate a best fit. The shipboard age model for Site U1338 provided initial guide tie points for the Match software (TP1–TP6) (supporting information Table S2b).

A depth (Site U1338) to age (Site 982) correlation was generated using four benthic foraminiferal records: (1) $\delta^{18}O_{\_5pt}$, (2) $\delta^{13}C$, (3) filtered $\delta^{18}O_{\_400\text{-}kyr}$, and (4) filtered $\delta^{13}C_{\_400\text{-}kyr}$. The filtered $\delta^{18}O_{\_400\text{-}kyr}$ and $\delta^{13}C_{\_400\text{-}kyr}$ were generated in Analyseries using a 0.0025 Gaussian filter (bandwidth 0.002) [*Paillard et al*., 1996] to aid alignment of the long-term trend. The $\delta^{18}O_{\_5pt}$ data sets emphasizes orbital cycles <400 kyr while maximizing the signal-to-noise ratio. Where the $\delta^{18}O_{\_5pt}$ variability is reduced, the $\delta^{13}C$ data sets guide Match and enable correlation of globally synchronous $\delta^{13}C$ events (see supporting information Text S1 for details) [*Woodruff and Savin*, 1989; *Billups*, 2002; *Billups et al*., 2008].

2.4. Spectral Analyses

We conducted spectral analyses (wavelet and Blackman-Tukey) to establish the dominant frequencies and variability at Sites U1338 and 982 in depth, shipboard age, and refined age domains. We used this approach to determine that correlating Site U1338 to the astronomically tuned Site 982 target did not induce any artificial variations. Blackman-Tukey (B-Tukey) analyses of Site U1338 records used a Bartlett window on equally spaced (linear interpolation), linearly detrended, normalized to unit variance and prewhitened data sets [*Paillard et al*., 1996]. Frequencies >14 m/>570 kyr were removed to emphasize higher frequencies (Gaussian notch filter at 0.00; depth bandwidth 0.07; age bandwidth 0.00175). Wavelet analyses of the Sites U1338 and 982 records were generated using the expanded *Torrence and Compo* [1998] package [*Grinsted et al*., 2004].

2.5. Estimating Cryosphere and Carbon Cycle Sensitivity and Earth System Response to Solar Forcing

We employ wavelet analyses to investigate the evolution of benthic foraminiferal $\delta^{18}O$ and $\delta^{13}C$ variability in the late Miocene to early Pliocene. We use this variability to assess the sensitivity of the cryosphere and carbon cycle to changes in external radiative forcing and to provide a first-order estimate of climate system sensitivity. Benthic foraminiferal $\delta^{18}O$ reflects global ice volume and deep-sea temperature and thus cryosphere variability [*Shackleton and Opdyke*, 1973], while benthic $\delta^{13}C$ reflects the oceanic $\delta^{13}C_{DIC}$ reservoir and global carbon cycling [*Broecker and Peng*, 1982]. Increased cryosphere and carbon cycle sensitivity to radiative forcing should result in greater benthic foraminiferal $\delta^{18}O$ (cryosphere) and $\delta^{13}C$ (carbon cycle) variability, which corresponds to higher power in wavelet analyses. External radiative forcing is approximated using the combined eccentricity, obliquity (tilt), and precession solutions from the La2004 astronomical solution (ETP: eccentricity-tilt-precession) [*Paillard et al*., 1996; *Laskar et al*., 2004].

Published studies highlight the relationship between benthic foraminiferal $\delta^{18}O$ and obliquity amplitude modulation, with low-amplitude obliquity nodes associated with more positive $\delta^{18}O$ [*Turco et al*., 2001; *Westerhold et al*., 2005; *Pälike et al*., 2006]. Here we investigate how sensitively the cryosphere ($\delta^{18}O$) and the carbon cycle ($\delta^{13}C$) respond to changes in obliquity amplitude modulation, to establish whether either system experiences reduced sensitivity (e.g. an interval when the amplitudes of the response and the forcing do not correlate). As obliquity is the dominant forcing, we focus on the 30–50 kyr bandwidth to obtain a qualitative estimate of the sensitivity of major climatic systems (cryosphere and carbon cycle) to this high-latitude radiative forcing. We constructed a simplified qualitative obliquity forcing for the late Miocene to early Pliocene based on the strength in the obliquity bandwidth (30–50 kyr) in the wavelet analyses of the ETP curve. Qualitative $\delta^{18}O$ and $\delta^{13}C$ obliquity responses were constructed from wavelet analyses of the Sites U1338 and 982 stable isotope records. The simplified obliquity forcing and $\delta^{18}O$ and $\delta^{13}C$ responses were compared to obtain qualitative estimates of cryosphere ($\delta^{18}O$) and the carbon cycle ($\delta^{13}C$) sensitivities to radiative forcing. The Earth System Response (ESR), defined here as the combined response of the carbon cycle and the cryosphere to obliquity forcing, was estimated by comparing the simplified obliquity forcing to the $\delta^{18}O/\delta^{13}C$ responses and cryosphere/carbon cycle sensitivities.

3. Results

3.1. Site U1338 *C. mundulus* $\delta^{18}O$ and $\delta^{13}C$ Versus Depth

Long-term (>20 m/>1–1.5 Myr) *C. mundulus* $\delta^{18}O$ variability is generally low. The $\delta^{18}O$ values become 0.2‰ more negative between 186 and 175 m CCSF-A, 0.3‰ more positive between 175 and 125 m CCSF-A, and 0.2‰ more negative between 125 and 48 m CCSF-A (Figures 3c and 3d and Table 1b). Between 180 and 150 m CCSF-A, short-term (~2 m/~40 kyr) 0.3‰ $\delta^{18}O$ variations occur (Table 1a), while well-defined ~0.5‰ cycles are observed between 110 and 80 m CCSF-A.

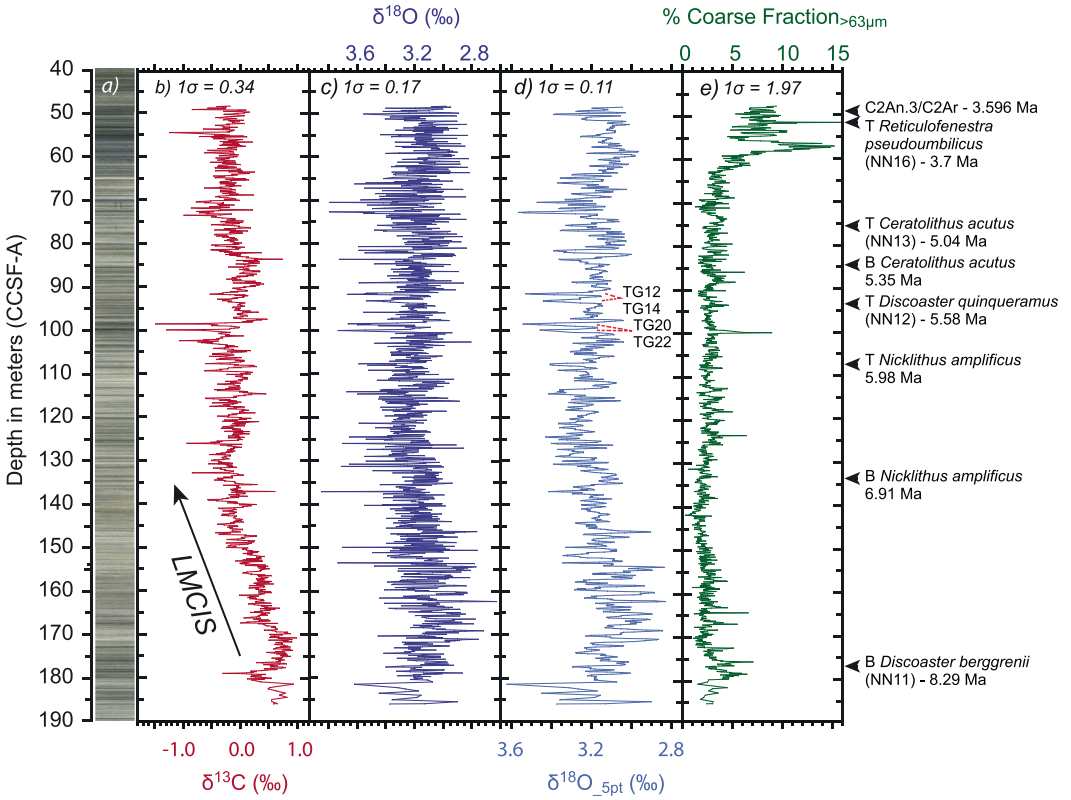

Figure 3. Overview of data generated from Site U1338. (a) Core photo [*Wilkens et al.*, 2013], benthic foraminiferal (*Cibicidoides mundulus*) (b) $\delta^{13}C$ and (c) $\delta^{18}O$, and (e) percentage coarse fraction (>63 µm). (d) The five-point weighted-moving-average $\delta^{18}O_{5pt}$ record of Figure 3c (weighting: first and fifth points = 30%; second and fourth points = 70%; third point = 100%). The nannofossil datums used for first-order shipboard age model are plotted on the right. The arrow in Figure 3b indicates the Late Miocene Carbon Isotope Shift (LMCIS).

The main feature of the *C. mundulus* $\delta^{13}C$ record is the 1‰ decrease between 170 and 130 m CCSF-A (Figure 3b and Table 1b), marking a permanent shift in the average $\delta^{13}C$ and corresponding to the globally recognized negative benthic foraminiferal $\delta^{13}C$ shift [*Keigwin*, 1979]. Up-section from the shift, long-term (>20/>1–1.5 Myr) 0.2‰ $\delta^{13}C$ oscillations occur. On average, short-term (~2 m/~40 kyr) $\delta^{13}C$ varies by 0.3–0.5‰ over the interval, with ~1‰ excursions occurring between 105 and 95 m CCSF-A. Throughout the record, the short-term $\delta^{18}O$ and $\delta^{13}C$ cycles are antiphased (Figure 3).

3.2. Match-Based Age Model

Based on the initial Match alignment, the long-term alignment of the Sites U1338 and 982 records is good, in particular, in the $\delta^{18}O$ records between 6.0 and 3.5 Ma and in the $\delta^{13}C$ records between 5.5 and 8.0 Ma (see supporting information Text S1). Short-term $\delta^{18}O_{5pt}$ and $\delta^{13}C$ variations are also well aligned, except where the shipboard-datum-based tie points forced an offset between similar isotopic excursions. Thus, we exchanged the shipboard-datum-based tie points for isotopic-excursion-based tie points. Depth offsets between the original and new isotope tie points are smaller than the depth error associated with the original shipboard datums (supporting information Table S1c). The second-generation Match age model (hereafter referred to as the refined age model, Figure 2) uses these adapted tie points. The long-term alignment is largely unaltered (Figure 4), and short-term correlation remains good, with distinct improvement associated with replacement tie points (Table S4 and supporting information Text S1).

Using our refined age model, sedimentation rates at Site U1338 vary considerably (Figure 2b) but are similar to shipboard age model estimates (Figure 2b) and comparable to those at Site 982 (10–150 m/Myr) [*Hodell et al.*, 2001]. Differences between the refined and shipboard age model-derived sedimentation rates prior to 6.5 Ma result from the improved alignment of the globally synchronous LMCIS event between Sites

Table 1. Stable Isotope Marine Isotope Stages (MIS) and Long-Term (>1 Myr) Trends

a) New marine isotope stage identification: 7.1-7.4 Ma[a]

Identifier	Type	Age (Ma)[b]
M-T-O2	Interglacial	7.163
M-T-O3	Glacial	7.181
M-T-O4	Interglacial	7.205
M-T-O5	Glacial	7.223
M-T-O6	Interglacial	7.241
M-T-O7	Glacial	7.262
M-T-O8	Interglacial	7.283
M-T-O9	Glacial	7.304
M-T-O10	Interglacial	7.322
M-T-O11	Glacial	7.340
M-T-O12	Interglacial	7.358

b) Long-term oxygen (O) and carbon (C) isotope trends[c]

Name	Identifier	Type	Depth Range[d]	Age Range[b]
Early Pliocene Oxygen Isotope Low	EPOL	O	48–70 m	3.5–4.8 Ma
Miocene-Pliocene Oxygen Isotope Low	MPOL	O	72–105 m	4.9–5.9 Ma
Messinian Oxygen Isotope High	MOH	O	105–150 m	5.9–7.0 Ma
Tortonian-Messinian Oxygen Isotope Low	TMOL	O	150–180 m	7.0–8.0 Ma
Late Miocene Carbon Isotope Shift	LMCIS	C	130–170 m	6.6–7.6 Ma

[a]Eleven new marine isotope stages are identified in the U1338 and 982 benthic foraminiferal $\delta^{18}O$ records from 7.4 to 7.1 Ma. The prefix M-T-O is used, as the stages are identified in the $\delta^{18}O$ record close to the Tortonian-Messinian boundary (~7.249 Ma) (see supporting information).
[b]Age (Ma) is reported on timescale from Site 982 [*Hodell et al.*, 2001], based on the La93 astronomical solution.
[c]Long-term $\delta^{18}O$ and $\delta^{13}C$ trends.
[d]Depth is given in m CCSF-A [*Wilkens et al.*, 2013].

U1338 and 982 [*Keigwin*, 1979; *Haq et al.*, 1980; *Hodell and Venz-Curtis*, 2006]. Between 6.5 and 3.5 Ma, we identify 30 marine isotope stages [*Shackleton et al.*, 1995; *Lisiecki and Raymo*, 2005; *van der Laan et al.*, 2005] in the Site U1338 $\delta^{18}O$ record, including the prominent late Miocene TG12/14 and TG20/22 glaciations (see supporting information Text S2). In addition, we identify 11 new global marine isotope stages between

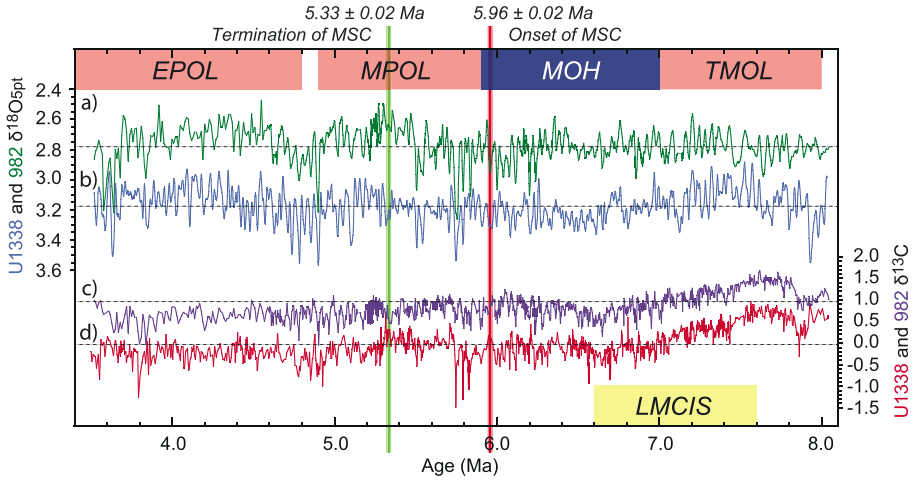

Figure 4. Isotope record overview on age. Benthic $\delta^{18}O_{\_5pt}$ and $\delta^{13}C$ records from sites (b and d) U1338 and (a and c) 982 on the second-generation Match age scale. Pink bars indicate intervals of reduced long-term benthic $\delta^{18}O$, coupled with higher $\delta^{18}O$ variability: the Early Pliocene (EPOL), the Miocene-Pliocene (MPOL), and the Tortonian-Messinian (TMOL) Oxygen Isotope Lows. The purple bar indicates intervals of increased long-term benthic $\delta^{18}O$, coupled with reduced $\delta^{18}O$ variability: Messinian Oxygen Isotope High (MOH). A yellow bar indicates the LMCIS. The MSC onset (red line) and termination (green line) with associated ages [*Krijgsman et al.*, 1999] are also shown. See also Table 1b. The dotted lines are placed at the averages for each record and aided identification of long-term oxygen maxima and minima.

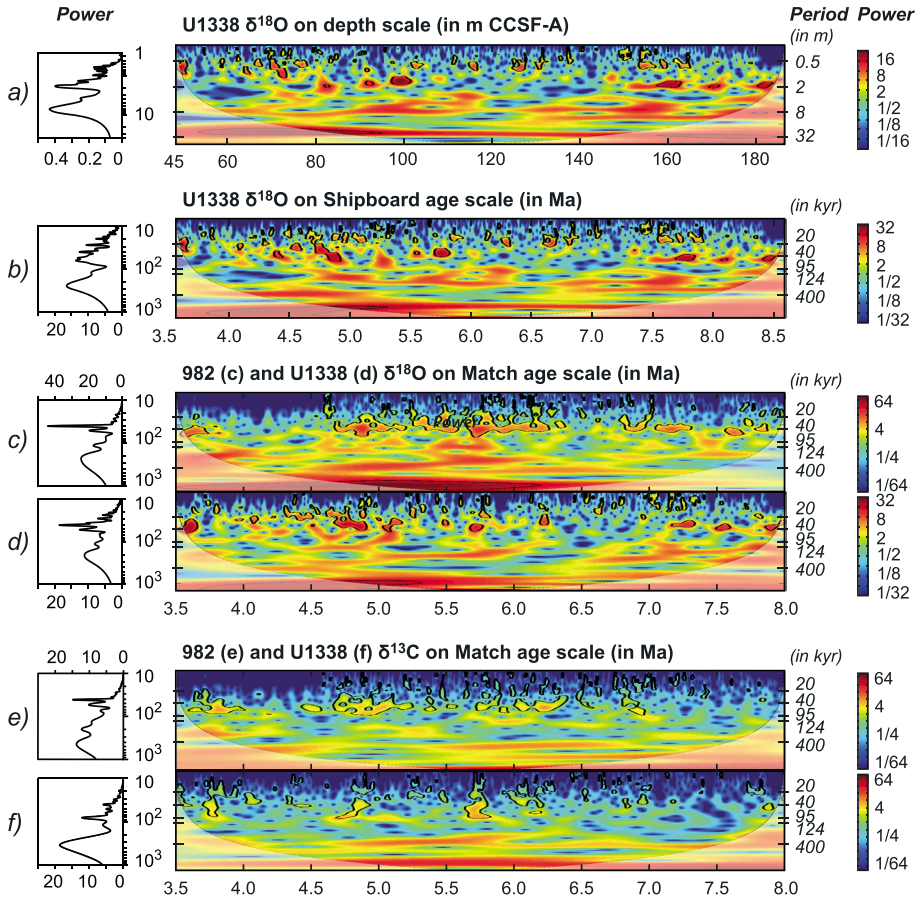

Figure 5. Spectral analyses for sites U1338 and 982. The left-hand side shows the B-Tukey spectra, with the corresponding wavelet analyses on the right: Site U1338 $\delta^{18}O$ on (a) depth, (b) shipboard age, and (c and d) the second-generation Match age scales with the Site 982 data, and (e and f) benthic $\delta^{13}C$ on the Match age scale for both sites (Site 982 data from *Hodell et al.* [2001]). Numbers on the vertical axes are in kiloyears for the age spectra and in meters for depth spectra. The software package includes 95% confidence limits (black lines) around significant power, and an opaque area shows the cone of influence, where edge effects due to data set length are present.

7.4 and 7.1 Ma, based on well-defined $\delta^{18}O$ excursions (~0.3‰) found in the Sites U1338 and 982 benthic foraminiferal $\delta^{18}O$ records (Table 1a and supporting information Text S2). Due to a reduction in $\delta^{18}O$ variability and signal-to-noise ratio at both sites, the refined age model from 7.0 and 6.5 Ma should be treated cautiously.

To determine if the Match correlation between Sites U1338 and 982 has induced any artificial cyclicity into the Site U1338 records, we compared the power distribution pattern in the depth, shipboard, and refined age model domains. This comparison reveals distinct patterns shared by the three wavelets, irrespective of domain (see Figures 5a–5d for U1338 $\delta^{18}O$). Power shifts from a broader 40–60 kyr bandwidth in the shipboard spectra to a narrower 40–50 kyr bandwidth in the refined age spectra. However, the broader shipboard bandwidth likely reflects changes in U1338 sedimentation rates that are not captured by the low-resolution nature of the shipboard age model. Similarities between the spectra suggest a lack of artificial cyclicity in the Site U1338 record and support our hypothesis that the refined age model wavelets reflect the true isotopic response. This observation indicates that the Match wavelets can be used to reconstruct background climate variability and Earth System Response (ESR) to external radiative forcing.

3.3. Spectral Analysis

The B-Tukey analyses of Site U1338 $\delta^{18}O$ reveal that obliquity is the dominant forcing and is visible throughout most of the record as 1.5–2.0 m cycles in the depth spectra (Figure 5a) and broad band of high power around 40–65 kyr in the shipboard age spectra (Figure 5b) and around 40–50 kyr in the refined age spectra (Figure 5d). The $\delta^{18}O$ wavelet analyses confirm obliquity dominance (Figures 5a–5d). However, obliquity is reduced in the

early Messinian. All spectral analyses of $\delta^{18}O$ indicate that strong 200 kyr and ~1.0–1.2 Myr cycles are present (Figures 5a–5d).

Site U1338 $\delta^{13}C$ spectral analyses also reveal obliquity, which is visible as 2.0 m cycles, as a broad band of power at 40–50 kyr in the shipboard age spectra, and ~40 kyr in the refined age spectra (Figure 5f). Dominant power in the $\delta^{13}C$ records occurs at 70 kyr (shipboard) and 80 kyr (refined), which may reflect a multiple of the 40 kyr obliquity cycle, if every second 40 kyr cycle has a larger amplitude, as is observed in some intervals (Figure 5f). The wavelet analyses of Sites U1338 and 982 $\delta^{13}C$ confirm the dominance of obliquity, except in the earliest part of the record (8.0–6.3 Ma; Figures 5e and 5f). $\delta^{13}C$ also displays a strong long-term eccentricity cycle throughout. At both sites, precession variability is minor and not continuous.

4. Discussion

4.1. Defining a Late Miocene to Early Pliocene Isotope Stratigraphy: Long-Term Trends and New Global Marine Isotope Stages

The new *C. mundulus* $\delta^{18}O$ and $\delta^{13}C$ records from Site U1338 are the first high-resolution continuous stable isotope records from the Pacific Ocean that span the 8.0 to 3.5 Ma interval and resolve all orbital-scale cycles. As such, these records enable refinement of the global late Miocene isotope stratigraphy. Site U1338 reveals more positive absolute $\delta^{18}O$ and more negative $\delta^{13}C$ values than the Site 982 records (Figure 4). The $\delta^{18}O$ difference likely reflects temperature offsets between the sites resulting from differences in water depth and source region (modern day: depth difference: ~ 3 km; temperature difference: ~ 2°C) [*Locarnini et al.*, 2010]. The intersite $\delta^{13}C$ difference may reflect water mass aging and suggests a North Atlantic source during this time interval [*Broecker and Peng*, 1982; *Wright et al.*, 1991; *Hodell and Venz-Curtis*, 2006; *Klevenz et al.*, 2008].

On the basis of our new alignment, several long-term (>1 Myr) trends can be identified in the Sites U1338 and 982 benthic foraminiferal $\delta^{18}O$ records, implying global and synchronous change (Figure 4 and Table 1b). For example, the Tortonian-Messinian Oxygen Isotope Low (TMOL, 8–7 Ma) displays more negative average benthic foraminiferal $\delta^{18}O$, coupled with distinct obliquity-driven fluctuations. The Messinian Oxygen Isotope High (MOH, 7–5.9 Ma) is characterized by the most positive long-term benthic $\delta^{18}O$ values, particularly at Site U1338, and a distinct reduction in obliquity-driven variability. The Miocene-Pliocene Oxygen Isotope Low (MPOL, 5.9–4.9 Ma) displays more negative average benthic foraminiferal $\delta^{18}O$ and increased obliquity-driven variability and is followed by a brief ~100–200 kyr interval of more positive $\delta^{18}O$, which occurs during a long-term eccentricity minimum. Long-term benthic foraminiferal $\delta^{18}O$ decreases during the Early Pliocene Oxygen Isotope Low (EPOL; 4.8–3.5 Ma). Although obliquity-driven variability is reduced during the EPOL, this observation may be biased by lower Pliocene sedimentation rates at Sites 982 and U1338.

4.2. Constraining Late Miocene to Early Pliocene Climate Variability and Earth System Response

Comparison of the spectral analyses from Sites U1338 and 982 (Figure 5) to ETP forcing (Figure 6a) reveals the dominance of obliquity forcing over this interval [*Mix et al.*, 1995; *Pisias et al.*, 1995; *Shackleton et al.*, 1995; *Hodell et al.*, 2001; *Bickert et al.*, 2004]. While high power is present in the ~40–50 kyr bandwidth in the Sites U1338 and 982 isotope records, power is absent from the precession bandwidth at Site 982 and is negligible at Site U1338, suggesting that precession has minimal influence on both these high- and low-latitude benthic isotope records.

Long-term $\delta^{18}O$ variability at Sites U1338 and 982 is visible as high power in the 200–250 kyr band, which is not strongly represented in the ETP forcing (Figure 6a). The Site U1338 $\delta^{18}O$ wavelet also has power in the 30 kyr band, which is also recognized in Pleistocene, Pliocene, and late Miocene records [*Pisias and Rea*, 1988; *Mix et al.*, 1995; *Shackleton et al.*, 1995; *Lisiecki and Raymo*, 2005; *Lourens et al.*, 2010]. In the Pleistocene, high 30 kyr power is attributed to a nonlinear climate interaction between the 40 kyr obliquity and quasi 100 kyr eccentricity cycle [*Pisias and Rea*, 1988; *Huybers and Wunsch*, 2004, 2005]. However, 100 kyr cycles are not observed in late Miocene to Pliocene isotope records. Spectral analysis of obliquity reveals a weak secondary peak at ~29 kyr; however, a direct climate response is unlikely [*Laskar et al.*, 2004]. *Lourens et al.* [2010] attributes ~30 kyr power in the late Pliocene to a nonlinear climate response to obliquity (e.g. the sum frequency of the 41 kyr obliquity signal and its multiples, 82 kyr and 124 kyr, introduces a ~30 kyr beat). As obliquity dominates the Site U1338 records, the ~30 kyr power may reflect this nonlinear response. However,

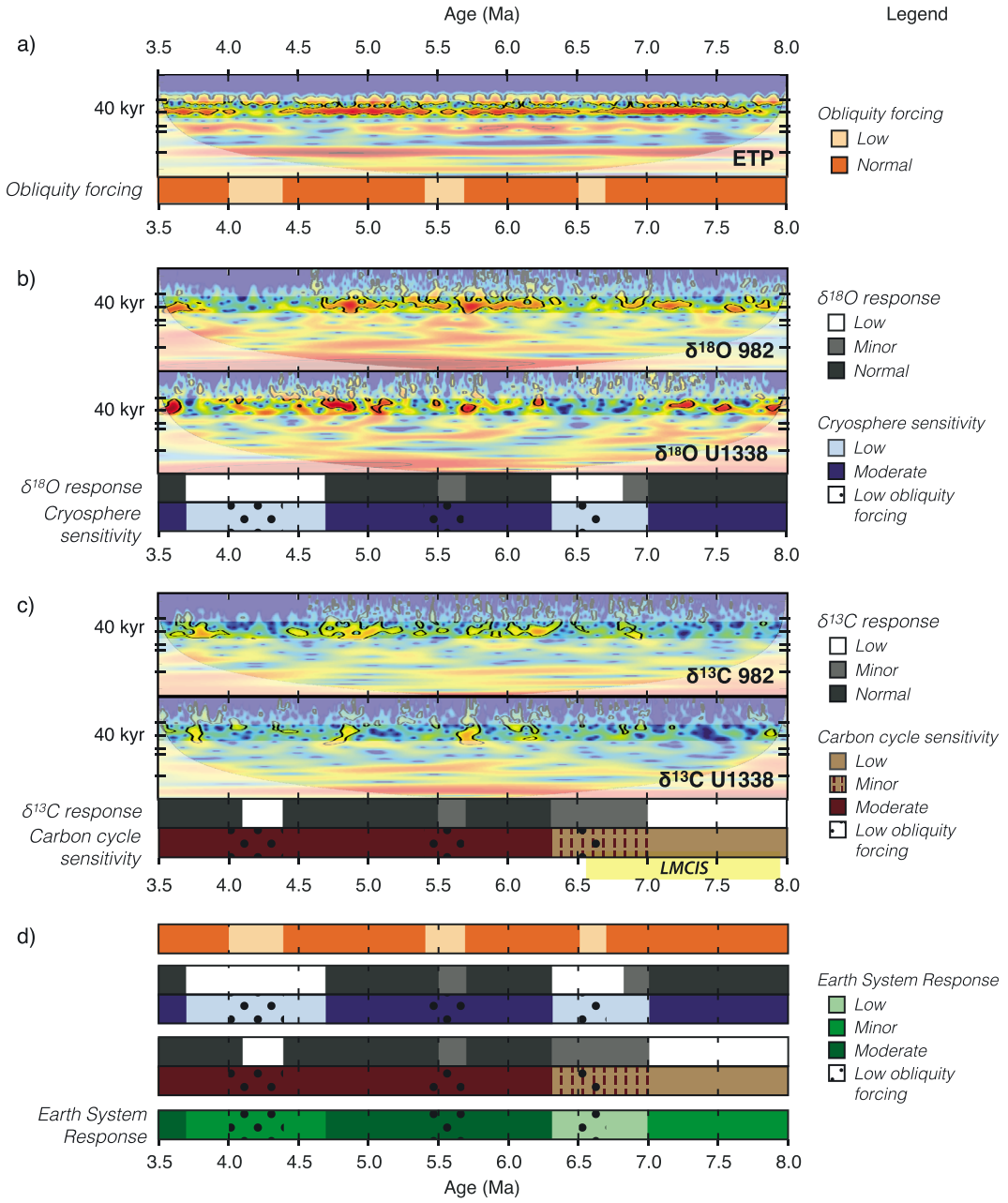

Figure 6. Sensitivity and response reconstructions. Simplified and qualitative (a) solar obliquity forcing and (b and c) stable isotope responses for Sites U1338 and 982 are shown (see legends), based on the highlighted obliquity bandwidth (30–50 kyr) in the wavelet analyses. The simplified isotope responses are compared to the simplified forcing to construct qualitative cryosphere ($\delta^{18}O$) and carbon cycle ($\delta^{13}C$) sensitivities (see text). (d) All five qualitative interpretations are compared to assess the Earth System Response (ESR). A moderate ESR is defined as intervals when both the cryosphere and carbon cycle are sensitive to obliquity forcing, whereas a low ESR is defined as intervals when neither components are sensitive to external forcing. The intervals defined as having a minor ESR reflect times when only one component was sensitive to obliquity forcing.

because the 30 kyr power is absent at Site 982, we cannot exclude the possibility of age model-induced artifacts in the Site U1338 spectra.

Wavelet analyses of $\delta^{13}C$ reveal that in addition to high power in the 40 kyr band at Sites U1338 and 982, high power is also observed in the 80 kyr and 120 kyr bands at Site U1338, which may reflect eccentricity forcing. However, because the period differs from the 95 kyr eccentricity forcing (Figure 6a) and our sampling resolution and record length are sufficient to distinguish between 80 kyr and 94 kyr cycles, we suggest that the

power in the 80 and 120 kyr bands at ~3.7, 4.7, and 5.7 Ma may be an expression of amplitude variability in the 41 kyr cycle (Figure 5f). Previous studies reveal that power in the ~81 and ~123 kyr bands appears when every second or third obliquity cycle is larger in amplitude than surrounding cycles [*Lourens et al*., 2010]. We observe well-defined variable-amplitude obliquity cycles in the Site U1338 $\delta^{13}C$ record (Figure 4d), during the intervals when high 80 and 120 kyr power is observed in the wavelet analyses (Figure 5f).

Site U1338 and 982 $\delta^{13}C$ records also show a strong response to long-term eccentricity throughout the late Miocene-early Pliocene, as has been previously documented for the Oligocene and early to middle Miocene [*Woodruff and Savin*, 1985; *Zachos et al*., 1997; *Pälike et al*., 2006; *Holbourn et al*., 2013]. A strong 400 kyr cycle is observed in benthic $\delta^{13}C$ records across the middle Miocene and related to the expansion of Antarctic ice sheets [*Holbourn et al*., 2005, 2007, 2013; *Shevenell et al*., 2008]. Similarly, *De Boer et al*. [2014] found strong coherence at 400 kyr between modeled ice volume and benthic foraminiferal $\delta^{13}C$ records throughout the Plio- and Pleistocene, which is attributed to ice sheet control of long-term carbon cycling. The presence of strong 400 kyr cycle in the late Miocene to early Pliocene $\delta^{13}C$ spectra supports the hypothesis for long-term Antarctic ice volume control of global carbon cycling, as ice-proximal records also indicate ice sheet fluctuations at this time [*Monien et al*., 2012; *Ohneiser et al*., 2015].

The strong obliquity forcing dominating the late Miocene to early Pliocene records at Sites U1338 and 982 suggests high-latitude forcing of global climate, as changes in tilt affect the seasonal contrast most at high latitudes. Comparing obliquity forcing in the ETP wavelet to the dominant obliquity response in the benthic foraminiferal $\delta^{18}O$ (cryosphere) and the $\delta^{13}C$ (carbon cycle) wavelets will enable us to approximate the cryosphere and the carbon cycle sensitivity to external solar forcing.

4.2.1. Assessing Cryosphere and Carbon Cycle Sensitivity to Obliquity Forcing

To assess cryosphere sensitivity, we constructed a simplified obliquity forcing and $\delta^{18}O$ response. Simplified obliquity forcing is qualitatively evaluated as either low or normal obliquity forcing (orange bar, Figure 6a). The $\delta^{18}O$ response is evaluated as low, minor, or moderate (black bar, Figure 6b), depending on whether significant power (defined by 95% confidence limits in the wavelet analyses; black lines, Figure 6) is present in the obliquity bandwidth of neither (low), one (minor), or both (moderate) of the Sites U1338 and 982 $\delta^{18}O$ wavelets. We assume that the benthic $\delta^{18}O$ signal reflects changes in ice volume and not temperature. This assumption is supported by low-resolution benthic foraminiferal Mg/Ca-derived bottom water temperature records from 8.0 to 3.5 Ma [*Billups and Schrag*, 2003; *Lear et al*., 2003, 2015]. Cryosphere sensitivity (blue bar, Figure 6b) is finally established by comparing the forcing level (orange bar) to the $\delta^{18}O$ response level (black bar), with low sensitivity occurring when the forcing is high, but the $\delta^{18}O$ response is low. Three intervals of moderate sensitivity occur (before ~7.0 Ma, from 6.3 to 4.7 Ma, and from 3.7 to 3.5 Ma) when obliquity forcing and $\delta^{18}O$ response are similar. During the two intervals of low sensitivity (7.0 to 6.3 Ma and 4.7 to 3.7 Ma), the lack of $\delta^{18}O$ response exceeds the interval of reduced obliquity forcing.

The benthic foraminiferal $\delta^{13}C$ response (black bar, Figure 6c) and carbon cycle sensitivity (brown bar, Figure 6c) were constructed similarly. An interval of moderate carbon cycle sensitivity exists from 6.3 to 3.5 Ma when the combined $\delta^{13}C$ response agrees well with obliquity forcing. However, as the power in the $\delta^{13}C$ wavelet analyses is not high, the coupling between carbon cycling and insolation is weak, suggesting that the benthic foraminiferal $\delta^{13}C$ variations are driven by climate system feedbacks, including interglacial/glacial cycles. The carbon cycle sensitivity is low before 7.0 Ma and minor between 7.0 and 6.3 Ma, coincident with the LMCIS. These first-order qualitative assessments of cryosphere and carbon cycle sensitivity are qualitatively confirmed by comparing the instantaneous amplitude of obliquity isolated from both the stable isotope records and the ETP curve (see supporting information Text S3).

4.2.2. Earth System Response to Obliquity Forcing

The Earth System Response (ESR) estimates the combined response of the $\delta^{18}O$ and $\delta^{13}C$ isotope systems as proxies for the cryosphere and carbon cycle response to external radiative forcing (green bar, Figure 6d). The ESR is a compilation of simplified obliquity forcing, $\delta^{18}O$ and $\delta^{13}C$ responses, and cryosphere and carbon cycle sensitivities. The ESR is moderate when forcing is present and the cryosphere or carbon cycle sensitivities is moderate, and low when sensitivities are low. ESR is minor when only the cryosphere or the carbon cycle sensitivity is moderate but the other is low. During low or absent obliquity forcing (dotted regions, Figure 6), the response is inferred from surrounding intervals and should be treated cautiously.

The ESR is moderate from 6.3 to 4.7 Ma and after 3.7 Ma, minor before 7.0 Ma and from 4.6 to 3.6 Ma, and low from 7.0 to 6.3 Ma. The minor response between 4.6 and 3.6 Ma coincides with reduced cryosphere sensitivity despite evidence that the carbon cycle responded to obliquity forcing. The minor response before 7.0 Ma is likely related to low carbon cycle sensitivity during the LMCIS, as the cryosphere remains sensitive during this interval.

No evidence exists for an amplified response to external radiative forcing between 8.0 and 3.5 Ma, suggesting a lack of high sensitivity intervals. The absence of high sensitivity and dominance of moderate to low sensitivity to external radiative forcing may have contributed to the long-term cryosphere stability inferred from late Miocene to early Pliocene benthic foraminiferal $\delta^{18}O$ records. This lack of sensitivity indicates that the coupling of the cryosphere and carbon cycle was not strong, despite the major LMCIS carbon cycle perturbation inferred from benthic foraminiferal $\delta^{13}C$ records (Figure 4d).

4.3. Late Miocene to Pliocene Isotope Stratigraphy and Reconstructed Climate Sensitivities: Implications for Global Climate Evolution

4.3.1. Late Miocene to Early Pliocene Ice Volume Dynamics

The low-amplitude ~1 Myr variability found in the Site U1338 benthic foraminiferal $\delta^{18}O$ record (Figure 4b) supports previous suggestions of cryosphere stability during the late Miocene and early Pliocene [*Hodell and Kennett*, 1986; *Hodell et al*., 1994, 2001; *Shackleton et al*., 1995; *Mix et al*., 1995; *Shackleton and Hall*, 1997; *Billups et al*., 1998, 2008; *Billups*, 2002; *Vidal et al*., 2002; *Bickert et al*., 2004; *Hodell and Venz-Curtis*, 2006]. However, obliquity-paced ice volume variations are implied by 40 kyr variability in the Pacific Site U1338 benthic foraminiferal $\delta^{18}O$ record and the anti-phase $\delta^{18}O$-$\delta^{13}C$ relationship characteristic of Pleistocene glacial-interglacial cycles (Figure 4) [*Shackleton*, 1977; *Broecker and Peng*, 1986]. The 40 kyr variability is particularly pronounced and dominant during the intervals between 7.4 and 7.0 Ma and 5.9 to 3.5 Ma (Table 1a and supporting information Text S2).

A compilation of published ice sheet-proximal sequences is shown in Figure 7a, together with benthic foraminiferal $\delta^{18}O$ records from major oceanic basins, the cryosphere sensitivity, and ESR estimates. These records reveal dynamic and stable climatic intervals during the late Miocene to early Pliocene (climate states are schematically represented in Figure 8a). Dynamic climate intervals have higher cryosphere sensitivity within long-term benthic foraminiferal $\delta^{18}O$ minima and short-term $\delta^{18}O$ variations. The stable climate interval has lower cryosphere sensitivity within long-term benthic foraminiferal $\delta^{18}O$ maxima and reduced short-term $\delta^{18}O$ variations.

Cryosphere sensitivity is moderate during the Tortonian-Messinian and Miocene-Pliocene Oxygen Isotope Lows (Figure 7a and Table 1b). Ice-proximal West Antarctic Ice Sheet (WAIS) records show evidence for proximal ice to shelf ice conditions before 7.6 Ma, implying that more negative benthic $\delta^{18}O$ during the Tortonian-Messinian oxygen isotope low likely reflects decreased global ice volumes [*McKay et al*., 2009; *Monien et al*., 2012]. Likewise, during the Miocene-Pliocene and Early Pliocene Oxygen Isotope Lows, proximal WAIS records suggest that dynamic ice shelf conditions initially prevailed and later gave way to open marine conditions, indicative of reduced ice volumes [*Monien et al*., 2012]. Evidence from Wilkes Land (IODP Site U1361) indicates repeated glacial retreat of the East Antarctic Ice Sheet during warmer intervals in the early Pliocene [*Cook et al*., 2013]. Therefore, the more negative deep-sea benthic foraminiferal $\delta^{18}O$ values of the Miocene-Pliocene and Early Pliocene Oxygen Isotope Lows likely reflect reduced global ice volumes.

The 40 kyr cyclicity observed in our benthic foraminiferal $\delta^{18}O$ records during the late Miocene to early Pliocene may reflect obliquity-driven ice sheet variations and/or deep-sea temperature fluctuations. We suggest that the well-defined variability during the Miocene-Pliocene Oxygen Isotope Low likely reflects dynamic Antarctic ice volume fluctuations, as reported in the Ross Sea during the early Pliocene [*Naish et al*., 2009] (Figure 7a). The dominant 40 kyr benthic foraminiferal $\delta^{18}O$ variability of the Tortonian-Messinian Oxygen Isotope Low may also indicate earlier dynamic obliquity-driven ice sheet variability (Figures 4 and 7a). Although the Early Pliocene Oxygen Isotope Low coincides with low cryosphere sensitivity interval (4.7 to 3.7 Ma), obliquity-modulated ice sheet variability is recognized in Antarctic continental marginal sequences [*Naish et al*., 2009] (Figure 7a). Thus, reduced cryosphere sensitivity indicated by the deep-sea isotopic records may reflect the lower temporal sampling resolution in Site U1338 (~7.5 kyr) and Site 982 (~10 kyr) [*Hodell and Venz-Curtis*, 2006] early Pliocene records. Finally, the brief (100–200 kyr) interval of increased average benthic foraminiferal $\delta^{18}O$ from 4.8 to 4.9 Ma coincides with a very long (2.4 Myr) eccentricity minimum and may reflect an interval of increased global

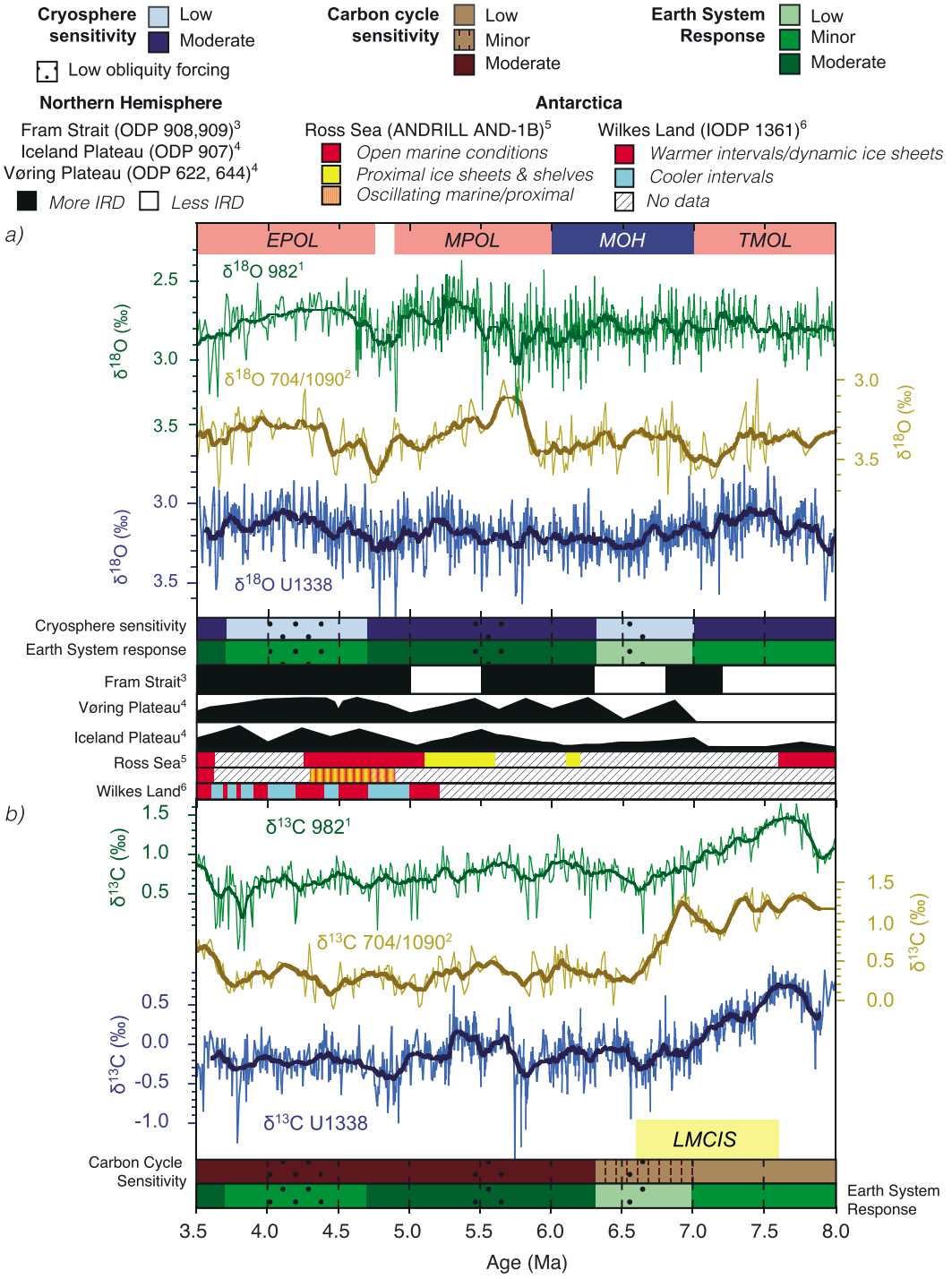

Figure 7. Climate evolution overview. A comparison is made of isotope records and proximal ice records from the Northern and Southern Hemispheres, including (a) $\delta^{18}O$ and (b) $\delta^{13}C$ records from several sites (Figure 1). The long-term carbon and oxygen isotope trends (Figure 4 and Table 1b), cryosphere and carbon cycle sensitivity, and Earth System Response (Figure 6) are also shown. The thick line in all isotope records is the 100 kyr average. The Southern Ocean is represented by combined records from ODP sites 704 and 1090, which have been correlated to the Atlantic site 982 [*Müller et al.*, 1991; *Hodell and Venz*, 1992; *Fronval and Jansen*, 1996; *Wolf-Welling et al.*, 1996; *Venz and Hodell*, 2002; *Hodell and Venz-Curtis*, 2006; *Naish et al.*, 2009; *Monien et al.*, 2012; *Cook et al.*, 2013].

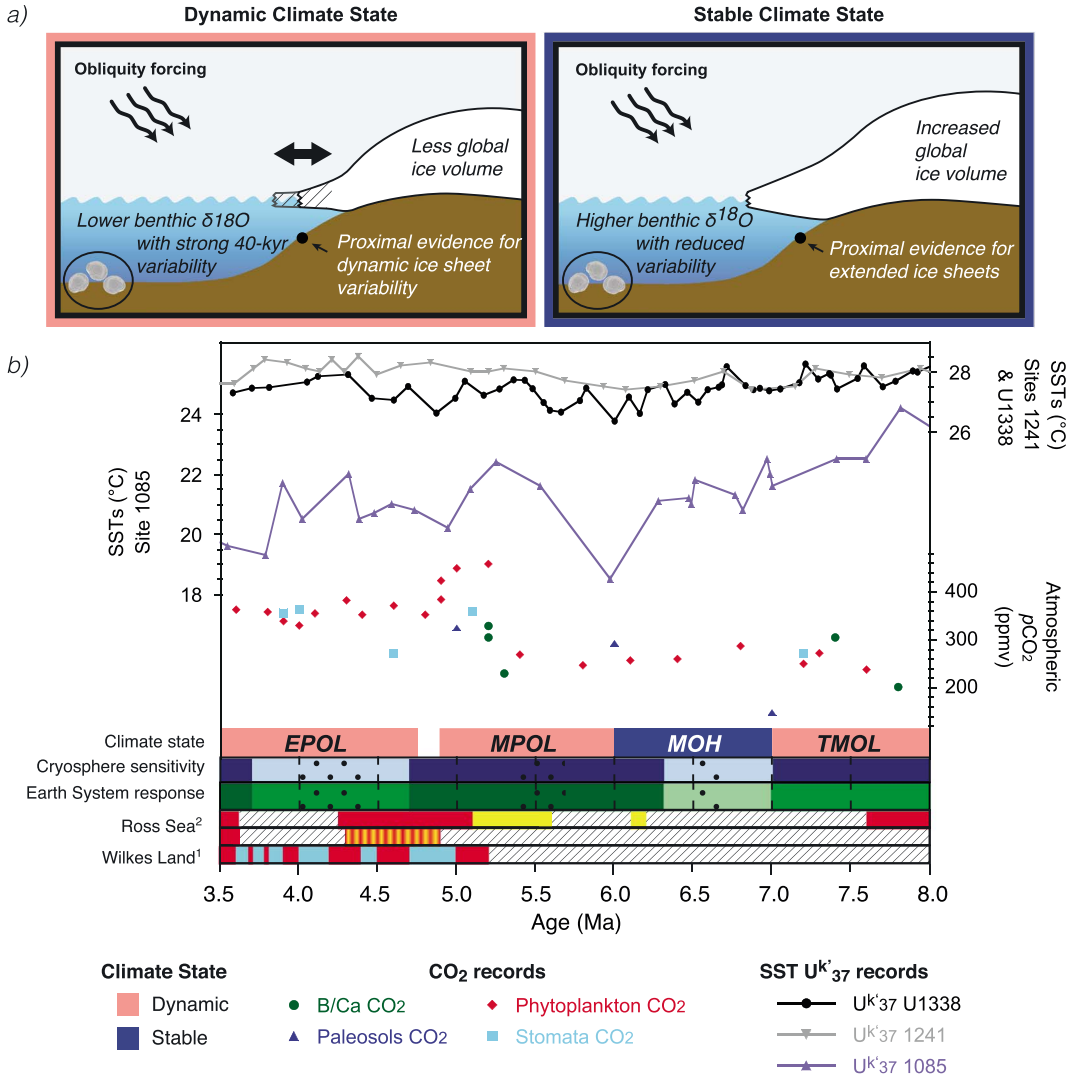

Figure 8. Climate state overview. (a) Schematic representation of the dynamic and stable climate states occurring during the late Miocene to early Pliocene is given together with (b) an overview of sea surface temperatures and atmospheric CO_2 records for this period and the salient features of Figure 7 (same legend applies). The dynamic (pink box) and stable climate (purple box) states are shown (EPOL, etc., Figure 4) [*Fronval and Jansen*, 1996; *Wolf-Welling et al.*, 1996; *Naish et al.*, 2009; *Beerling and Royer*, 2011 and the references therein; *Rommerskirchen et al.*, 2011; *Monien et al.*, 2012; *Seki et al.*, 2012; *Cook et al.*, 2013; *Rousselle et al.*, 2013].

ice volume driven by low seasonality. However, the benthic foraminiferal $\delta^{18}O$ records still display 40 kyr variability during this interval, suggesting that cryosphere sensitivity to obliquity is not reduced.

The Messinian Oxygen Isotope High is associated with a relatively stable climatic state, with reduced cryosphere sensitivity and increased long-term and reduced short-term benthic $\delta^{18}O$ foraminiferal variability (Figure 7a). The Messinian Oxygen Isotope High was coeval with increases in ice-rafted debris around Greenland [*Fronval and Jansen*, 1996; *Wolf-Welling et al.*, 1996] and evidence of alternating warmer-colder conditions with extended WAIS ice shelves [*Monien et al.*, 2012]. Additionally, proximal records from the Antarctic margin indicated increased ice volume at this time [*Ohneiser et al.*, 2015]. Thus, the more positive benthic $\delta^{18}O$ of the Messinian Oxygen Isotope High may reflect cooling and ice growth in the Northern and Southern Hemispheres. Reduced $\delta^{18}O$ variability indicates that the deglaciation threshold increased during the Messinian Oxygen Isotope High.

The shift between a dynamic and stable climatic state correlates with overall global ice volume trends (Figure 8a). The stable state, with reduced ice sheet variability and cryosphere sensitivity, coincides with increased ice

volume, whereas the dynamic state, with higher ice sheet variability and cryosphere sensitivity, occurs during times of reduced ice volume. Hence, ice extent (e.g. proximity to the continental shelf edge) may be important for determining cryosphere sensitivity to obliquity forcing. Ice sheets may reach equilibrium during periods of increased ice volume, thereby making the system less sensitive to forcing. When ice volume is reduced, dynamic ice sheet variations indicate restoration of cryosphere sensitivity. Enhanced ice-albedo feedbacks or thermal inertia of the ocean may also explain the reduction in sensitivity during intervals of increased ice volume [*Hansen et al*., 2011; *Qu and Hall*, 2014].

Global ice volume changes may reflect changes in temperature and/or atmospheric pCO_2 levels. During the late Miocene to early Pliocene, atmospheric pCO_2 is relatively low [*Pagani et al*., 1999; *Kürschner et al*., 2008; *Seki et al*., 2010; *Tipple and Pagani*, 2010] (Figure 8b). Although a ~100 ppmv increase in atmospheric pCO_2 occurs around the Miocene-Pliocene boundary, there is no coeval decrease in benthic $\delta^{18}O$, implying a relatively weak coupling between pCO_2 and ice volume at this time. *Cook et al*. [2013] suggested that dynamic ice sheets were associated with relatively warm Southern Ocean sea surface temperatures (SSTs) during the Pliocene. Similarly, warm SSTs occur in the Pacific and South Atlantic Oceans [*Rommerskirchen et al*., 2011; *Seki et al*., 2012; *Rousselle et al*., 2013] during dynamic climate intervals and lower SSTs during the stable climate interval between 7.0 and 5.9 Ma (Figure 8b). These observations, coupled with our new analyses, suggest that dynamic late Miocene ice sheets may also be associated with intervals of warmer Southern Ocean SSTs.

4.3.2. Messinian Salinity Crisis

During the Messinian Salinity Crisis (MSC), the Mediterranean basin was isolated from the Atlantic Ocean [*Hsu et al*., 1973; *Krijgsman et al*., 1999, 2010]. The high-resolution benthic $\delta^{18}O$ records from Sites U1338 and 982 suggest that glacio-eustatic control on the onset of the MSC was minimal. The onset (red line, Figure 4) coincides with TG32 (see supporting information Text S2) and the more positive $\delta^{18}O$ of the Messinian Oxygen Isotope High, providing deep-sea distal evidence supporting ice-proximal evidence for increased ice volume [*Ohneiser et al*., 2015]. However, neighboring events, TG20 and TG22 (~5.7–5.8 Ma, Figure 3), are larger than TG32, making a strong glacio-eustatic control on the exact timing of the MSC onset unlikely.

The termination of the MSC occurs during the Miocene-Pliocene Oxygen Isotope Low, which is characterized by more negative benthic foraminiferal $\delta^{18}O$, reduced global ice volume, dynamic ice sheets, and moderate cryosphere sensitivity (Figure 7a) [*Naish et al*., 2009; *Cook et al*., 2013]. This long-term reduced ice volume supports reconstructions that higher sea level around the Miocene-Pliocene boundary contributed to the reflooding of the Mediterranean basin (Figure 4) [*Miller et al*., 2005; *Ohneiser et al*., 2015]. However, at Sites U1338 and 982, the MSC termination (green line, Figure 4) coincides with a small short-lived $\delta^{18}O$ maximum (~0.25–0.3‰), suggesting that the exact timing of the MSC termination may not be controlled by glacio-eustacy, in contrast to the interpretation of *Ohneiser et al*. [2015]. This disagreement possibly originates from amplitude differences of the MSC termination $\delta^{18}O$ maximum at the different locations: ~0.25–0.3‰ at Sites U1338 and 982 compared with the 0.53‰ signal observed at ODP Site 846 [*Ohneiser et al*., 2015]. Independent high-resolution temperature estimates are required to constrain the relative temperature and ice volume contributions to the deep-sea benthic foraminiferal $\delta^{18}O$ signal.

4.3.3. Late Miocene Carbon Isotope Shift

The Late Miocene Carbon Isotope Shift (LMCIS) is a globally synchronous event [*Keigwin*, 1979; *Haq et al*., 1980; *Hodell and Venz-Curtis*, 2006]. Proposed forcing mechanisms include a global shift in the $\delta^{13}C$ of oceanic dissolved inorganic carbon ($\delta^{13}C_{DIC}$) [*Hodell et al*., 1994, 2001; *Bickert et al*., 2004; *Hodell and Venz-Curtis*, 2006] or a large-scale surface ocean productivity event [*Grant and Dickens*, 2002; *Diester-Haass et al*., 2004, 2005, 2006]. Although evidence exists for a large-scale biogenic bloom in the equatorial Pacific and other regions during the LMCIS [*Grant and Dickens*, 2002; *Diester-Haass et al*., 2005; *Expedition 320/321 Scientists*, 2010; *Pälike et al*., 2010; *Lyle et al*., 2012; *Lyle and Baldauf*, 2015], the similar timing (~7.5–6.5 Ma) and magnitude of the LMCIS in Pacific, North Atlantic, and Southern Ocean records supports the oceanic $\delta^{13}C_{DIC}$ hypotheses (Figure 7b).

The LMCIS coincides with the low carbon cycle sensitivity identified between 8 and 7 Ma (Figures 6c and 7b) and suggests that the coupling between insolation and the carbon cycle broke down and that a process independent of solar forcing perturbed the carbon system. A change in continental carbon flux (including riverine and weathering input) or in the fractionation of organic matter in the surface ocean [*Kump and Arthur*, 1999; *Bickert et al*., 2004] or a change in the air-sea CO_2 exchange [*Hodell and Venz-Curtis*, 2006] could alter oceanic $\delta^{13}C_{DIC}$. The late Miocene global C_3:C_4 vegetation shift, coincident with the LMCIS, may have

driven an increased flux of ^{12}C-enriched material into the ocean [*Pagani et al*., 1999]. It may also have permanently altered the ^{12}C fractionation coefficient into marine organic matter (Δ_{org}) and driven a permanent −1‰ excursion in $\delta^{13}C_{DIC}$ [*Kump and Arthur*, 1999]. A decrease in ocean-atmosphere CO_2 exchange driven by increased sea ice extent is proposed to explain the distinct shape of the LMCIS in the Southern Ocean (ODP 704/1090, Figure 7b) [*Hodell and Venz-Curtis*, 2006]. However, *Waddell et al*. [2009] found no evidence for Southern Ocean stratification during the LMCIS. Furthermore, the reduced carbon cycle sensitivity during the LMCIS coincides with an interval where the cryosphere responds strongly to obliquity (Figure 6b). If the LMCIS was driven by reduced air-sea CO_2 exchange due to increased sea ice cover, a similarly strong response to obliquity forcing in the $\delta^{13}C$ record would be expected; however, this is not present (Figure 6c). Overall, low carbon cycle sensitivity during the LMCIS supports hypotheses for a change in the continental carbon flux into the oceans or in the Δ_{org}, for instance, through increased C_4 vegetation input into the surface ocean [*Kump and Arthur*, 1999; *Pagani et al*., 1999; *Bickert et al*., 2004].

5. Conclusions

New *C. mundulus* $\delta^{18}O$ and $\delta^{13}C$ records from IODP Site U1338 are the first high-resolution Pacific Ocean records between 8.0 and 3.5 Ma with sufficient resolution to resolve orbital-scale variability. Stratigraphic correlation to ODP Site 982 (North Atlantic) enables identification of 11 new marine isotope stages between 7.4 and 7.1 Ma. Additionally, four long-term global trends are identified in benthic $\delta^{18}O$: (1) the Tortonian-Messinian Oxygen Isotope Low from 8 to 7 Ma; (2) the Messinian Oxygen Isotope High from 7 to 5.9 Ma; (3) the Miocene-Pliocene Oxygen Isotope Low from 5.9 to 4.9 Ma; and (4) and the Early Pliocene Oxygen Isotope Low from 4.8 to 3.5 Ma.

Obliquity-driven variability dominates the Pacific and North Atlantic benthic foraminiferal $\delta^{18}O$ and $\delta^{13}C$ records except during the Messinian oxygen isotope high. We qualitatively assess the wavelet analyses of the Pacific and North Atlantic isotope records to define cryosphere and carbon cycle sensitivity to obliquity forcing. An Earth System Response (ESR), estimated by combining the cryosphere and carbon cycle sensitivities, shows distinct regimes of low, minor, and moderate response to obliquity forcing. The ESR, cryosphere, and carbon cycle sensitivities indicate a weak coupling of the cryosphere and the carbon cycle during the late Miocene to early Pliocene. We suggest that the presence of low response intervals, and the absence of high sensitivity intervals, contributed to the late Miocene to early Pliocene climate stability.

Our records also provide insight into the timing and occurrence of the MSC and the LMCIS. The MSC occurs during the Miocene-Pliocene oxygen isotope low. The characteristic low average benthic foraminiferal $\delta^{18}O$ and strong obliquity-driven variability of this interval suggests that generally reduced ice volume and higher sea level contributed to the MSC termination. The LMCIS coincides with an interval of reduced carbon cycle sensitivity, suggesting that the driver of this event is independent of solar insolation changes.

Dynamic and stable climatic states were identified in the late Miocene to early Pliocene. The dynamic state dominates this interval and is characterized by moderate ESR and cryosphere sensitivity, with obliquity-driven Antarctic ice sheet variations. A stable state dominated during the Messinian Oxygen Isotope High, characterized by reduced ESR and cryosphere sensitivity, extended Antarctic ice sheets, and increasing Greenland ice-rafted debris. The reduction in orbital-scale ice sheet variability during the stable climate state compared with the dynamic state implies a higher glaciation-deglaciation threshold during the stable state. The dynamic and stable climatic states correspond to periods of reduced and extended global ice volume, respectively. Correlations between the dynamic state and warmer SSTs suggest an important role for oceanic heat in late Miocene to early Pliocene Antarctic cryosphere evolution.

Acknowledgments

Samples were provided by the Integrated Ocean Drilling Program (IODP) and the IODP Gulf Coast Repository (GCR). The R/V *JOIDES Resolution* Expedition 320/321 science party members are acknowledged for their effort in collecting the material used in this study. S. Davis, D. Ostermann, and S. Robinson are thanked for their help and guidance in the laboratory. D. Hodell is thanked for his suggestions and fruitful discussions about the age model. T. Kluge, T. van de Flierdt, B. Wade, and T. Westerhold are thanked for providing constructive and critical feedback that helped this work. M. Lyle and a second anonymous reviewer are thanked for their invaluable suggestions, which helped improve this manuscript. A.J. Drury was funded by a Janet Watson studentship from Imperial College London, and the isotope work was partially facilitated by a European Consortium for Ocean Research Drilling (ECORD) research grant received by A.J. Drury in 2012. All data are available at Paleoceanography as supporting information and on Pangaea (http://doi.pangaea.de/10.1594/PANGAEA.856679).

References

Beerling, D. J., and D. L. Royer (2011), Convergent Cenozoic CO_2 history, *Nat. Geosci.*, *4*(7), 418–420, doi:10.1038/ngeo1186.

Bickert, T., G. H. Haug, and R. Tiedemann (2004), Late Neogene benthic stable isotope record of Ocean Drilling Program Site 999: Implications for Caribbean paleoceanography, organic carbon burial, and the Messinian Salinity Crisis, *Paleoceanography*, *19*, PA1023, doi:10.1029/2002PA000799.

Billups, K. (2002), Late Miocene through early Pliocene deep water circulation and climate change viewed from the sub-Antarctic South Atlantic, *Palaeogeogr. Palaeoclimatol. Palaeoecol.*, *185*(3–4), 287–307, doi:10.1016/s0031-0182(02)00340-1.

Billups, K., and D. P. Schrag (2003), Application of benthic foraminiferal Mg/Ca ratios to questions of Cenozoic climate change, *Earth Planet. Sci. Lett.*, *209*(1–2), 181–195, doi:10.1016/s0012-821x(03)00067-0.

Billups, K., A. Ravelo, and J. Zachos (1998), Early Pliocene deep water circulation in the western equatorial Atlantic: Implications for high-latitude climate change, *Paleoceanography*, *13*(1), 84–95, doi:10.1029/97PA02995.
Billups, K., C. Kelly, and E. Pierce (2008), The late Miocene to early Pliocene climate transition in the Southern Ocean, *Palaeogeogr. Palaeoclimatol. Palaeoecol.*, *267*(1–2), 31–40, doi:10.1016/J.Palaeo.2008.05.013.
Broecker, W., and T. Peng (1982), *Tracers in the Sea*, Lamont-Doherty Earth Observ., Palisades, N. Y.
Broecker, W. S., and T.-H. Peng (1986), Carbon cycle: 1985—Glacial to interglacial changes in the operation of the global carbon cycle, *Radiocarbon*, *28*(2), 309–327.
Cook, C. P., et al. (2013), Dynamic behaviour of the East Antarctic Ice Sheet during Pliocene warmth, *Nat. Geosci.*, *6*(9), 765–769, doi:10.1038/ngeo1889.
de Boer, B., L. J. Lourens, and R. S. W. van de Wal (2014), Persistent 400,000-year variability of Antarctic ice volume and the carbon cycle is revealed throughout the Plio-Pleistocene, *Nat. Commun.*, *5*, 2999, doi:10.1038/ncomms3999.
Diester-Haass, L., P. A. Meyers, and T. Bickert (2004), Carbonate crash and biogenic bloom in the late Miocene: Evidence from ODP Sites 1085, 1086, and 1087 in the Cape Basin, southeast Atlantic Ocean, *Paleoceanography*, *19*, PA1007, doi:10.1029/2003PA000933.
Diester-Haass, L., K. Billups, and K. C. Emeis (2005), In search of the late Miocene-early Pliocene "biogenic bloom" in the Atlantic Ocean (Ocean Drilling Program Sites 982, 925, and 1088), *Paleoceanography*, *20*, PA4001, doi:10.1029/2005PA001139.
Diester-Haass, L., K. Billups, and K. C. Emeis (2006), Late Miocene carbon isotope records and marine biological productivity: Was there a (dusty) link?, *Paleoceanography*, *21*, PA4216, doi:10.1029/2006PA001267.
Drury, A. J., G. P. Lee, G. M. Pennock, and C. M. John (2014), Data report: Late Miocene to early Pliocene coccolithophore and foraminiferal preservation at Site U1338 from scanning electron microscopy, in *Proceedings of the Integrated Ocean Drilling Program*, vol. 320/321, edited by H. Pälike et al., Integr. Ocean Drilling Program Manage. Int., Inc, Tokyo.
Expedition 320/321 Scientists (2010), Site U1338, in *Proceedings of the Integrated Ocean Drilling Program*, vol. 320/321, edited by H. Pälike et al.
Fronval, T., and E. Jansen (1996), Late Neogene paleoclimates and paleoceanography in the Iceland-Norwegian Sea: Evidence from the Iceland and Vøring Plateaus, *Proc. Ocean Drill. Program*, *151*, 455–468.
Grant, K. M., and G. R. Dickens (2002), Coupled productivity and carbon isotope records in the southwest Pacific Ocean during the late Miocene-early Pliocene biogenic bloom, *Palaeogeogr. Palaeoclimatol. Palaeoecol.*, *187*(1–2), 61–82, doi:10.1016/s0031-0182(02)00508-4.
Grinsted, A., J. C. Moore, and S. Jevrejeva (2004), Application of the cross wavelet transform and wavelet coherence to geophysical time series, *Nonlinear Process. Geophys.*, *11*(5–6), 561–566.
Hansen, J., M. Sato, P. Kharecha, and K. Von Schuckmann (2011), Earth's energy imbalance and implications, *Atmos. Chem. Phys.*, *11*(24), 13,421–13,449, doi:10.5194/acp-11-13421-2011.
Haq, B., T. Worsley, and L. Burckle (1980), Late Miocene marine carbon-isotopic shift and synchroneity of some phytoplanktonic biostratigraphic events, *Geology*, *8*, 427–431.
Hodell, D. A., and J. P. Kennett (1986), Late Miocene-early Pliocene stratigraphy and paleoceanography of the South Atlantic and southwest Pacific oceans: A synthesis, *Paleoceanography*, *1*(3), 285–311, doi:10.1029/PA001i003p00285.
Hodell, D. A., and K. A. Venz (1992), Toward a high-resolution stable isotopic record of the Southern Ocean during the Plio-Pleistocene (4.8 to 0.8 Ma), in *The Antarctic Paleoenvironment: A Perspective on Global Change Part I*, vol. 56, edited by J. P. Kennett and D. A. Warnke, pp. 265–310, AGU, Washington, D. C.
Hodell, D. A., and K. A. Venz-Curtis (2006), Late Neogene history of deepwater ventilation in the Southern Ocean, *Geochem. Geophys. Geosyst.*, *7*, Q09001, doi:10.1029/2005GC001211.
Hodell, D. A., R. H. Benson, D. V. Kent, A. Boersma, and K. R. E. Bied (1994), Magnetostratigraphic, biostratigraphic, and stable-isotope stratigraphy of an upper Miocene drill core from the Sale-Briqueterie (northwestern Morocco)—A high-resolution chronology for the Messinian stage, *Paleoceanography*, *9*(6), 835–855, doi:10.1029/94PA01838.
Hodell, D. A., J. H. Curtis, F. J. Sierro, and M. E. Raymo (2001), Correlation of late Miocene to early Pliocene sequences between the Mediterranean and North Atlantic, *Paleoceanography*, *16*(2), 164–178, doi:10.1029/1999PA000487.
Holbourn, A., W. Kuhnt, M. Schulz, and H. Erlenkeuser (2005), Impacts of orbital forcing and atmospheric carbon dioxide on Miocene ice-sheet expansion, *Nature*, *438*(7067), 483–487, doi:10.1038/nature04123.
Holbourn, A., W. Kuhnt, M. Schulz, J. A. Flores, and N. Andersen (2007), Orbitally-paced climate evolution during the middle Miocene "Monterey" carbon-isotope excursion, *Earth Planet. Sci. Lett.*, *261*(3–4), 534–550, doi:10.1016/j.epsl.2007.07.026.
Holbourn, A., W. Kuhnt, S. Clemens, W. Prell, and N. Andersen (2013), Middle to late Miocene stepwise climate cooling: Evidence from a high-resolution deep water isotope curve spanning 8 million years, *Paleoceanography*, *28*, 688–699, doi:10.1002/2013PA002538.
Hsu, K. J., W. B. F. Ryan, and M. B. Cita (1973), Late Miocene desiccation of the Mediterranean, *Nature*, *242*(5395), 240–244.
Huybers, P., and C. Wunsch (2004), A depth-derived Pleistocene age model: Uncertainty estimates, sedimentation variability, and nonlinear climate change, *Paleoceanography*, *19*, PA1028, doi:10.1029/2002PA000857.
Huybers, P., and C. Wunsch (2005), Obliquity pacing of the late Pleistocene glacial terminations, *Nature*, *434*(7032), 491–494.
Jansen, E., and M. E. Raymo (1996), Leg 162: New frontiers on past climates, in *Proceedings of the Ocean Drilling Program, Initial Rep.*, vol. 162, edited by E. Jansen et al., pp. 5–20, Ocean Drilling Program, College Station, Tex.
Keigwin, L. D. (1979), Late Cenozoic stable isotope stratigraphy and paleoceanography of DSDP sites from the east equatorial and central North Pacific Ocean, *Earth Planet. Sci. Lett.*, *45*(2), 361–382, doi:10.1215/03616878-2682650.
Klevenz, V., D. Vance, D. N. Schmidt, and K. Mezger (2008), Neodymium isotopes in benthic foraminifera: Core-top systematics and a down-core record from the Neogene South Atlantic, *Earth Planet. Sci. Lett.*, *265*(3–4), 571–587, doi:10.1016/j.epsl.2007.10.053.
Krijgsman, W., F. J. Hilgen, I. Raffi, F. J. Sierro, and D. S. Wilson (1999), Chronology, causes and progression of the Messinian Salinity Crisis, *Nature*, *400*, 652–655, doi:10.1038/23231.
Krijgsman, W., M. Stoica, I. Vasiliev, and V. V. Popov (2010), Rise and fall of the Paratethys Sea during the Messinian Salinity Crisis, *Earth Planet. Sci. Lett.*, *290*(1–2), 183–191, doi:10.1016/j.epsl.2009.12.020.
Kump, L. R., and M. A. Arthur (1999), Interpreting carbon-isotope excursions: Carbonates and organic matter, *Chem. Geol.*, *161*(1–3), 181–198, doi:10.1016/s0009-2541(99)00086-8.
Kürschner, W. M., Z. Kvacek, and D. L. Dilcher (2008), The impact of Miocene atmospheric carbon dioxide fluctuations on climate and the evolution of terrestrial ecosystems, *Proc. Natl. Acad. Sci. U.S.A.*, *105*(2), 449–453, doi:10.1073/pnas.0708588105.
Laskar, J., P. Robutel, F. Joutel, M. Gastineau, A. C. M. Correia, and B. Levrard (2004), A long-term numerical solution for the insolation quantities of the Earth, *Astron. Astrophys.*, *428*(1), 261–285, doi:10.1051/0004-6361:20041335.
Lear, C. H., Y. Rosenthal, and J. D. Wright (2003), The closing of a seaway: Ocean water masses and global climate change, *Earth Planet. Sci. Lett.*, *210*(3–4), 425–436, doi:10.1016/s0012-821x(03)00164-x.

Lear, C. H., H. K. Coxall, G. L. Foster, D. J. Lunt, E. M. Mawbey, Y. Rosenthal, S. M. Sosdian, E. Thomas, and P. A. Wilson (2015), Neogene ice volume and ocean temperatures: Insights from infaunal foraminiferal Mg/Ca paleothermometry, *Paleoceanography*, *30*, 1437–1454, doi:10.1002/2015PA002833.

Lisiecki, L. E., and T. D. Herbert (2007), Automated composite depth scale construction and estimates of sediment core extension, *Paleoceanography*, *22*, PA4213, doi:10.1029/2006PA001401.

Lisiecki, L. E., and P. A. Lisiecki (2002), Application of dynamic programming to the correlation of paleoclimate records, *Paleoceanography*, *17*(4), 1049, doi:10.1029/2001PA000733.

Lisiecki, L. E., and M. E. Raymo (2005), A Pliocene-Pleistocene stack of 57 globally distributed benthic delta O-18 records, *Paleoceanography*, *20*, PA1003, doi:10.1029/2004PA001071.

Locarnini, R. A., A. V. Mishonov, J. I. Antonov, T. P. Boyer, H. E. Garcia, O. K. Baranova, M. M. Zweng, and D. R. Johnson (2010), in *World Ocean Atlas 2009, Volume 1: Temperature*, *NOAA Atlas NESDIS 68*, vol. 1, edited by S. Levitus, 184 pp., U. S. Government Print. Off., Washington, D. C.

Lourens, L. J., J. Becker, R. Bintanja, F. J. Hilgen, E. Tuenter, R. S. W. van de Wal, and M. Ziegler (2010), Linear and non-linear response of late Neogene glacial cycles to obliquity forcing and implications for the Milankovitch theory, *Quat. Sci. Rev.*, *29*(1–2), 352–365, doi:10.1016/j.quascirev.2009.10.018.

Lyle, M., and J. Backman (2013), Data report: Calibration of XRF-estimated CaCO3 along the Site U1338 splice, in *Proceedings of the Integrated Ocean Drilling Program*, vol. 320, edited by H. Pälike et al., pp. 1–16, Integrated Ocean Drilling Program Management International, Inc., Tokyo.

Lyle, M., and J. Baldauf (2015), Biogenic sediment regimes in the Neogene equatorial Pacific, IODP Site U1338: Burial, production, and diatom community, *Palaeogeogr. Palaeoclimatol. Palaeoecol.*, *433*, 106–128, doi:10.1016/j.palaeo.2015.04.001.

Lyle, M., A. O. Lyle, T. Gorgas, A. Holbourn, T. Westerhold, E. Hathorne, K. Kimoto, and S. Yamamoto (2012), Data report: Raw and normalized elemental data along the Site U1338 splice from X-ray fluorescence scanning 1 X-ray fluorescence analytical technique, in *Proceedings of the Integrated Ocean Drilling Program*, *Sci. Results*, vol. 320/321, edited by H. Pälike et al., pp. 1–19, Integrated Ocean Drilling Program Management International, Inc., Tokyo.

Lyle, M. W., H. Pälike, H. Nishi, I. Raffi, K. Gamage, A. Klaus, and IODP Expeditions 320 and 321, Science Party, and Expedition 320/321 Scientists (2010), *The Pacific Equatorial Age Transect, IODP Expeditions 320 and 321: Building a 50-Million-Year-Long Environmental Record of the Equatorial Pacific Ocean*, *Sci. Drill.*, edited by H. Pälike et al., pp. 4–15, Integrated Ocean Drilling Program Management International, Inc., Tokyo.

McKay, R., et al. (2009), The stratigraphic signature of the late Cenozoic Antarctic Ice Sheets in the Ross Embayment, *Geol. Soc. Am. Bull.*, *121*(11–12), 1537–1561, doi:10.1130/b26540.1.

Miller, K. G., et al. (2005), The phanerozoic record of global sea-level change, *Science*, *310*, 1293–1298, doi:10.1126/science.1116412.

Mix, A. C., N. G. Pisias, W. Rugh, J. Wilson, A. Morey, and T. Hagelberg (1995), Benthic foraminiferal stable isotope record of Site 849 (0–5 Ma): Local and global climate changes, in *Proceedings of the Ocean Drilling Program*, *Sci. Results*, vol. 138, edited by N. G. Pisias et al., pp. 371–412, Ocean Drilling Program, College Station, Tex.

Monien, D., G. Kuhn, H. von Eynatten, and F. M. Talarico (2012), Geochemical provenance analysis of fine-grained sediment revealing Late Miocene to recent paleo-environmental changes in the Western Ross Sea, Antarctica, *Global Planet. Change*, *96–97*, 41–58, doi:10.1016/j.gloplacha.2010.05.001.

Müller, D. W., D. A. Hodell, and P. Ciesielski (1991), Late Miocene to earliest Pliocene (9.8–4.5 Ma) paleoceanography of the subantarctic southeast Atlantic: Stable isotopic, sedimentologic, and microfossil evidence, *Proc. Ocean Drill. Program, Sci. Results*, *114*, 459–474.

Naish, T., et al. (2009), Obliquity-paced Pliocene West Antarctic ice sheet oscillations, *Nature*, *458*(7236), 322–U84, doi:10.1038/nature07867.

Ohneiser, C., F. Florindo, P. Stocchi, A. P. Roberts, R. M. DeConto, and D. Pollard (2015), Antarctic glacio-eustatic contributions to late Miocene Mediterranean desiccation and reflooding, *Nat. Commun.*, *6*, 8765, doi:10.1038/ncomms9765.

Pagani, M., K. H. Freeman, and M. A. Arthur (1999), Late Miocene atmospheric CO_2 concentrations and the expansion of C-4 grasses, *Science*, *285*(5429), 876–879, doi:10.1126/science.285.5429.876.

Pagani, M., K. Caldeira, R. Berner, and D. J. Beerling (2009), The role of terrestrial plants in limiting atmospheric CO_2 decline over the past 24 million years, *Nature*, *460*(7251), 85–U94, doi:10.1038/nature08133.

Paillard, D., L. Labeyrie, and P. Yiou (1996), Macintosh program performs time-series analysis, *Eos Trans. AGU*, *77*(39), 379, doi:10.1029/96EO00259.

Pälike, H., R. D. Norris, J. O. Herrle, P. A. Wilson, H. K. Coxall, C. H. Lear, N. J. Shackleton, A. K. Tripati, and B. S. Wade (2006), The heartbeat of the Oligocene climate system, *Science*, *314*(5807), 1894–8, doi:10.1126/science.1133822.

Pälike, H., M. Lyle, H. Nishi, I. Raffi, K. Gamage, A. Klaus, and Expedition 320/321 Scientists (2010), Expedition 320/321 summary, in *Proceedings of the Integrated Ocean Drilling Program*, vol. 320, edited by H. Pälike et al., pp. 2–141.

Pälike, H., et al. (2012), A Cenozoic record of the equatorial Pacific carbonate compensation depth, *Nature*, *488*(7413), 609–14, doi:10.1038/nature11360.

Pisias, N. G., and D. K. Rea (1988), Late Pleistocene paleoclimatology of the central equatorial Pacific: Sea surface response to the southeast trade winds, *Paleoceanography*, *3*(1), 21–37, doi:10.1029/PA003i001p00021.

Pisias, N. G., L. A. Mayer, and A. C. Mix (1995), Paleoceanography of the eastern equatorial Pacific during the Neogene: Synthesis of Leg 138 drilling results, in *Proceedings of the Ocean Drilling Program*, *Sci. Results*, vol. 138, edited by N. G. Pisias et al., pp. 5–21, Ocean Drilling Program, College Station, Tex.

Qu, X., and A. Hall (2014), On the persistent spread in snow-albedo feedback, *Clim. Dyn.*, *42*(1–2), 69–81, doi:10.1007/s00382-013-1774-0.

Rohling, E. J., et al. (2012), Making sense of palaeoclimate sensitivity, *Nature*, *491*(7426), 683–691, doi:10.1038/nature11574.

Rommerskirchen, F., T. Condon, G. Mollenhauer, L. Dupont, and E. Schefuss (2011), Miocene to Pliocene development of surface and subsurface temperatures in the Benguela Current system, *Paleoceanography*, *26*, PA3216, doi:10.1029/2010PA002074.

Rousselle, G., C. Beltran, M. A. Sicre, I. Raffi, and M. De Rafelis (2013), Changes in sea-surface conditions in the equatorial Pacific during the middle Miocene-Pliocene as inferred from coccolith geochemistry, *Earth Planet. Sci. Lett.*, *361*, 412–421, doi:10.1016/j.epsl.2012.11.003.

Royer, D. L., M. Pagani, and D. J. Beerling (2012), Geobiological constraints on Earth system sensitivity to CO_2 during the Cretaceous and Cenozoic, *Geobiology*, *10*(4), 298–310, doi:10.1111/j.1472-4669.2012.00320.x.

Ryan, W. B. F., et al. (2009), Global multi-resolution topography synthesis, *Geochem. Geophys. Geosyst.*, *10*, Q03014, doi:10.1029/2008GC002332.

Seki, O., G. L. Foster, D. N. Schmidt, A. Mackensen, K. Kawamura, and R. D. Pancost (2010), Alkenone and boron-based Pliocene pCO(2) records, *Earth Planet. Sci. Lett.*, *292*(1–2), 201–211, doi:10.1016/j.epsl.2010.01.037.

Seki, O., D. N. Schmidt, S. Schouten, E. C. Hopmans, J. S. S. Damste, and R. D. Pancost (2012), Paleoceanographic changes in the eastern equatorial Pacific over the last 10 Myr, *Paleoceanography*, *27*, PA3224, doi:10.1029/2011PA002158.

Shackleton, N. J. (1977), Tropical rainforest history and equatorial Pacific carbonate dissolution cycles, in *The Fate of Fossil Fuel CO_2 in the Oceans*, edited by N. R. Anderson and A. Malahoff, pp. 401–428, Plenum Press, New York.

Shackleton, N. J., and M. A. Hall (1997), The late Miocene stable isotope record, Site 926, in *Proceedings of the Ocean Drilling Program*, *Sci. Results*, vol. 154, edited by N. J. Shackleton et al., pp. 367–373, Ocean Drilling Program, College Station, Tex.

Shackleton, N. J., and N. D. Opdyke (1973), Oxygen isotope and palaeomagnetic stratigraphy of equatorial pacific core V28-238: Oxygen isotope temperatures and ice volume on a 10^5 and 10^6 year scale, *Quat. Res.*, *55*(1), 39–55, doi:10.1016/0033-5894(73)90052-5.

Shackleton, N. J., M. A. Hall, and D. Pate (1995), Pliocene stable isotope stratigraphy of Site 846, in *Proceedings of the Ocean Drilling Program*, *Sci. Results*, vol. 138, edited by N. G. Pisias et al., pp. 337–355.

Shevenell, A. E., J. P. Kennett, and D. W. Lea (2008), Middle Miocene ice sheet dynamics, deep-sea temperatures, and carbon cycling: A Southern Ocean perspective, *Geochem. Geophys. Geosyst.*, *9*, Q02006, doi:10.1029/2007GC001736.

Shipboard Scientific Party Exp.162 (1996), Site 982, in *Proceedings of the Ocean Drilling Program*, *Initial Rep.*, vol. 162, edited by E. Jansen et al.

Tipple, B. J., and M. Pagani (2010), A 35 Myr North American leaf-wax compound-specific carbon and hydrogen isotope record: Implications for C-4 grasslands and hydrologic cycle dynamics, *Earth Planet. Sci. Lett.*, *299*(1–2), 250–262, doi:10.1016/j.epsl.2010.09.006.

Torrence, C., and G. P. G. P. Compo (1998), A practical guide to wavelet analysis, *Bull. Am. Meteorol. Soc.*, *79*(1), 61–78, doi:10.1175/1520-0477(1998)079<0061:apgtwa>2.0.co;2.

Turco, E., F. J. Hilgen, L. J. Lourens, N. J. Shackleton, and W. J. Zachariasse (2001), Punctuated evolution of global climate cooling during the late middle to early late Miocene: High-resolution planktonic foraminiferal and oxygen isotope records from the Mediterranean, *Paleoceanography*, *16*(4), 405–423, doi:10.1029/2000PA000509.

van der Laan, E., S. Gaboardi, F. J. Hilgen, and L. J. Lourens (2005), Regional climate and glacial control on high-resolution oxygen isotope records from Ain el Beida (latest Miocene, northwest Morocco): A cyclostratigraphic analysis in the depth and time domain, *Paleoceanography*, *20*, PA1001, doi:10.1029/2003PA000995.

van der Laan, E., E. Snel, E. De Kaenel, F. J. Hilgen, and W. Krijgsman (2006), No major deglaciation across the Miocene-Pliocene boundary: Integrated stratigraphy and astronomical tuning of the Loulja sections (Bou Regreg area, NW Morocco), *Paleoceanography*, *21*, PA3011, doi:10.1029/2005PA001193.

Venz, K. A., and D. A. Hodell (2002), New evidence for changes in Plio-Pleistocene deep water circulation from Southern Ocean ODP Leg 177 Site 1090, *Palaeogeogr. Palaeoclimatol. Palaeoecol.*, *182*(3–4), 197–220, doi:10.1016/s0031-0182(01)00496-5.

Vidal, L., T. Bickert, G. Wefer, and U. Röhl (2002), Late Miocene stable isotope stratigraphy of SE Atlantic ODP Site 1085: Relation to Messinian events, *Mar. Geol.*, *180*(1–4), 71–85, doi:10.1016/s0025-3227(01)00206-7.

Waddell, L. M., I. L. Hendy, T. C. Moore, and M. W. Lyle (2009), Ventilation of the abyssal Southern Ocean during the late Neogene: A new perspective from the subantarctic Pacific, *Paleoceanography*, *24*, PA3206, doi:10.1029/2008PA001661.

Westerhold, T., T. Bickert, and U. Röhl (2005), Middle to late Miocene oxygen isotope stratigraphy of ODP site 1085 (SE Atlantic): New constraints on Miocene climate variability and sea-level fluctuations, *Palaeogeogr. Palaeoclimatol. Palaeoecol.*, *217*(3–4), 205–222, doi:10.1016/j.palaeo.2004.12.001.

Wilkens, R. H., G. R. Dickens, J. Tian, J. Backman, and E. 320/321 Scientists (2013), Data report: Revised composite depth scales for Sites U1336, U1337, and U1338, in *Proceedings of the Integrated Ocean Drilling Program*, *Sci. Results*, edited by H. Pälike et al., pp. 1–158, Integrated Ocean Drilling Program Management International, Inc., Tokyo.

Wolf-Welling, T. C. W., M. Cremer, S. O. Connell, A. Winkler, J. Thiede, and S. O'Connell (1996), Cenozoic Arctic Gateway paleoclimate variability: Indications from changes in coarse-fraction composition, in *Proceedings of the Integrated Ocean Drilling Program*, *Sci. Results*, vol. 151, edited by J. Thiede et al., pp. 515–567, Ocean Drilling Program, College Station, Tex.

Woodruff, F., and S. M. Savin (1985), δ13C values of Miocene Pacific benthic foraminifera: Correlations with sea level and biological productivity, *Geology*, *13*(2), 119–122, doi:10.1130/0091-7613(1985)13<119:CVOMPB>2.0.CO;2.

Woodruff, F., and S. M. Savin (1989), Miocene deepwater oceanography, *Paleoceanography*, *4*(1), 87–140, doi:10.1029/PA004i001p00087.

Wright, J. D., K. G. Miller, and R. G. Fairbanks (1991), Evolution of modern deepwater circulation: Evidence from the late Miocene Southern Ocean, *Paleoceanography*, *6*(2), 275–290, doi:10.1029/90PA02498.

Zachos, J., M. Pagani, L. Sloan, E. Thomas, and K. Billups (2001), Trends, rhythms, and aberrations in global climate 65 Ma to present, *Science*, *292*(5517), 686–693, doi:10.1126/science.1059412.

Zachos, J. C., B. P. Flower, and H. Paul (1997), Orbitally paced climate oscillations across the Oligocene / Miocene boundary, *Nature*, *388*, 567–570.